

2-D Cluster Variation Method Free Energy: Fundamentals and Pragmatics

Alianna J. Maren

Northwestern University School of Professional Studies

Master of Science in Data Science Program

and

Themasis

Themasis Technical Report TR-2019-02v1 (ajm)

alianna.maren@northwestern.edu

alianna@aliannajmaren.com

Revision Date: 2019-09-17

Version 1

Abstract

Despite being invented in 1951 by R. Kikuchi, the 2-D Cluster Variation Method (CVM), has not yet received attention. Nevertheless, this method can usefully characterize 2-D topographies using just two parameters; the activation enthalpy and the interaction enthalpy. This Technical Report presents 2-D CVM details, including the dependence of the various configuration variables on the enthalpy parameters, as well as illustrations of various topographies (ranging from “scale-free-like” to “rich club-like”) that result from different parameter selection. The complete derivation for the analytic solution, originally presented simply as a result in Kikuchi and Brush (1967) is given here, along with careful comparison of the analytically-predicted configuration variables versus those obtained when performing computational free energy minimization on a 2-D grid. The 2-D CVM can potentially function as a secondary free energy minimization within the hidden layer of a neural network, providing a basis for extending node activations over time and allowing temporal correlation of patterns.

Keywords: cluster variation method; entropy; approximation methods; free energy; free energy minimization; artificial intelligence; neural networks; deep learning; statistical thermodynamics; brain networks; neural connectivity

1 Introduction and Overview

This Technical Report serves as both a tutorial and as essential reference material for anyone who wishes to work with the 2-D cluster variation method (CVM), originally devised by Kikuchi in 1951 [1], and then further advanced by Kikuchi and Brush (1967) [2].

The essential notion of the CVM is that we work with a more complex entropy expression within the free energy formalism for a system.

In a simple Ising model, the entropy S can be computed based on only the relative fraction of active units in a bistate system. That is, there are only two kinds of units; *active* ones in state **A**, where the fraction of these units is denoted x_1 , and *inactive* ones in state **B**, where the fraction of these units is denoted x_2 . (Of course, $x_1 + x_2 = 1.0$.)

In contrast to the simple entropy used in the basic Ising model, in the CVM approach, we expand the entropy term. The CVM entropy term considers not only the relative fractions of units in states **A** and **B**, but also a set of *configuration variables*. The configuration variables for a 2-D CVM system include, in addition to the usual activation of single units, also the fractional values of different kinds of nearest neighbor and next-nearest-neighbor pairs, along with six different kinds of triplets. (Section 3 describes the configuration variables in depth.)

Our entropy term now involves what are essentially *topographic* variables. That is, the location of one unit in conjunction with another now makes a substantial difference.

As a result, when we do free energy minimization to find an equilibrium configuration for a given system, we arrive at a 2-D CVM with certain characteristic topographic properties. While the exact activation of a specific unit (whether it is in state **A** or state **B**) can vary, each time a given system is brought to equilibrium, the overall values for the configuration variables should be consistent for a given set of enthalpy parameters.

These topographic patterns are worth our attention and interest.

Figure 1 illustrates an example, for where a manually-designed initial system on the LHS (Left-Hand-Side) has been brought to free energy equilibrium on the RHS (Right-Hand-Side).

The remaining sections will investigate this figure in more depth; this is presented here as an illustration of the kind of results obtained via free energy minimization in a 2-D CVM grid.

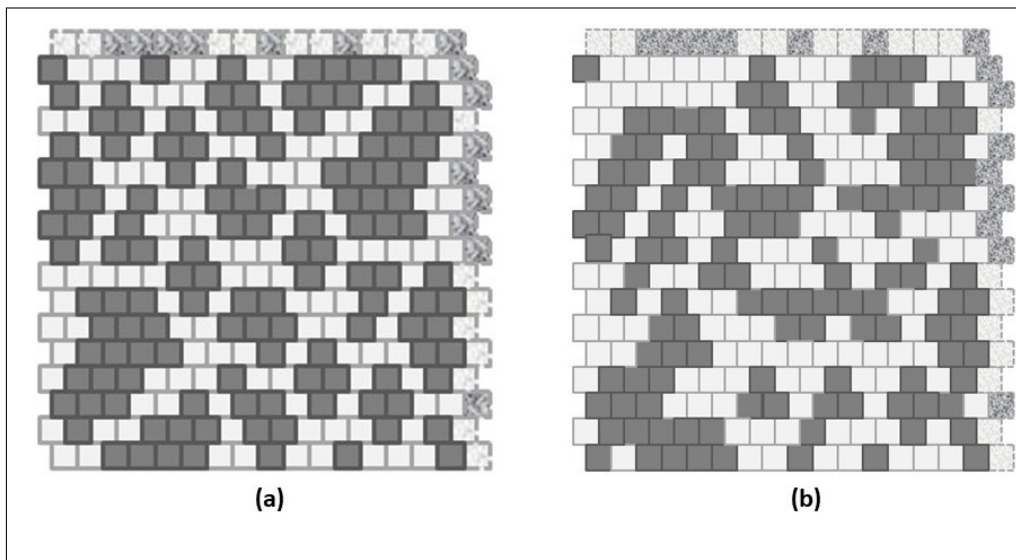


Figure 1: Illustration of (a) a manually-designed 2-D CVM grid that is (b) brought to a free energy equilibrium configuration.

Up until now, the CVM approach has not received a great deal of attention. However, as Figure 1 illustrates, this approach is potentially useful for characterizing 2-D systems that would naturally gravitate to a free energy-minimized state. Examples of potential applications include:

- *Modeling systems where the topography is an essential component of system description*; this can range from urban/rural topographies to brain images,
- *Providing an essential component of a new computational engine*, where *memories* of prior system states can persist over time, and
- *Providing the modeling component of a variational Bayes approach* that uses a *representational* system to model an *external* system, where the two are separated by a Markov blanket, and both systems are presumed to come to separate free energy equilibrium states.

The following Table 1 presents a glossary of the thermodynamic terms used in this Report.

Table 1: Thermodynamic Variable Definitions

Variable	Meaning
Activation enthalpy	Enthalpy ε_0 associated with a single unit (node) in the “on” or “active” state (A); influences configuration variables and is set to 0 in order to achieve an analytic solution for the free energy equilibrium
Configuration variable(s)	Nearest neighbor, next-nearest neighbor, and triplet patterns
Degeneracy	Number of ways in which a configuration variable can appear
Enthalpy	Internal energy H results from both per unit and pairwise interactions; often denoted H in thermodynamic treatments
Entropy	The entropy S is the distribution over all possible states; often denoted S in thermodynamic treatments and H in information theory
Equilibrium point	By definition, the free energy minimum for a closed system
Equilibrium distribution	Configuration variable values when free energy minimized for given h
Ergodic distribution	Achieved when a system is allowed to evolve over a long period of time
Free Energy	The thermodynamic state function F ; where $F = H-TS$; sometimes G is used instead of F ; referring to (thermodynamic) Gibbs free energy
<i>h-value</i>	A more useful expression for the interaction enthalpy parameter ε_1 ; $h = e^{2\beta\varepsilon_1}$, where $\beta = 1/k_\beta T$, and where k_β is Boltzmann’s constant and T is temperature; β can be set to 1 for our purposes
Interaction enthalpy	Between two unlike units, ε_1 ; influences configuration variables
Interaction enthalpy parameter	Another term for the <i>h-value</i> where $h = e^{2\varepsilon_1}$
Temperature	Temperature T times Boltzmann’s constant k_β is set equal to one

2 Background

The CVM approach is a useful and insightful way for describing systems in which the entropy is considered to be more than the relative proportion of “on” and “off” units. In short, the CVM approach allows

us to address the entropy of *patterns*, and not just the simple entropy of unit identification. Thus, it is somewhat surprising that the CVM is not yet well understood, and is not yet used more widely.

This section presents a brief historical overview, and identifies what may have been certain barriers to entry for researchers who might have otherwise considered this approach.

2.1 Evolution of the CVM applications

The primary applications of the CVM have, up until recently, predominantly been to computations of alloy phase diagrams as well as to studies of phase transitions in alloys. This application area was particularly dominant in the 1980's and 90's. For example, Sanchez et al. (1984) addressed the CVM's role in describing configurational thermodynamics (and specifically phase stability) of alloys [3], with a focus on the phenomenological and first principles theories of phase equilibrium. Maren et al. (1984) used a linear collection of 1-D CVMs to model phase transitions and hysteresis in a solid-state oxide [4].

In 1994, Sanchez and Becker reviewed this approach more comprehensively, focusing on how the 3-D CVM method could be used to construct the phase boundaries of solids (particularly alloys) [5]. Similarly, Pelizzola described the CVM for modeling Padé approximants and critical behaviour (1994) [6]. Within the same timeframe, Finel described how the CVM approach could generate reliable approximate results, comparing favorably with Monte Carlo methods [7], and Cirillo et al. (1996) used the 3-D CVM to describe the phase structure of the 3-D gonihedric Ising system [8].

This attention to how the CVM method could be used to describe 3-D systems continued into the 2000's. Kikuchi and Masuda-Jindoi (2002) extended the original method to include continuous atomic displacements within binary alloys [9]. This attention to how a 3-D CVM could describe the thermodynamic properties of alloys continued with work by Mohri (2013) [10].

Although the primary line of work from the 1980's through the early 2010's continued to be on applications of 3-D CVM models to alloys, some researchers began looking at the CVM in a more general context.

Beginning in the early 2000's, a few authors addressing general methods for machine learning and artificial intelligence included the CVM in their comprehensive reviews of methods. For example, Peliz-

zola broadened his earlier (1994) work to include the CVM in a more general treatment of probabilistic graph models (2005) [11]. Similarly, Yedidia et al. described the role of the CVM as one method for belief propagation (2002) [12]. Wainwright and Jordan included the CVM in their extensive monograph on graphical models, exponential families, and variational inference (2008) [13]. However, in all of these treatments, the CVM approach was included largely for completeness, and not as a primary method.

Practical applications, other than to metallurgy, have remained few up until now. Albers et al. used the CVM to study efficient linkage analysis on extended pedigrees (2006) [14], and Barton and Cocco (2013) used the CVM method (which they described as “selective cluster expansion”) to characterize neural structural and coding properties [15].

2.2 The CVM, neural networks, and brain science

While CVM applications to modeling 3-D systems such as alloys was dominant throughout the late 1990’s and early 2000’s, another (entirely different) application began to quietly take shape.

In the early 1990’s, Maren began evolving a new kind of CVM application. At that time, Maren was working in association with the Brain Research Center founded by Karl Pribram, who was then at Radford University, following a distinguished tenure at Stanford University [16]. Also, neural networks had recently emerged as a new computational force, and there was the potential to use neurophysiologically-based insights to further advance neural networks.

Within the intellectual fervor inspired by Pribram and colleagues, several community members realized that the statistical physics methods that already were the underpinnings for some neural networks (e.g., the Hopfield neural network and the Boltzmann machine) could play an even stronger role.

One of the challenging problems for neural networks, even then, was the difficulty making temporal associations and next-state predictions. The most well-known methods at that time were backpropagation-through-time and recurrent neural networks, both of which suffered deficiencies. A core factor underlying these deficiencies was that there was no way for a neural network to learn temporal associations that might be made over a longer time interval; both backpropagation-

through-time and recurrent neural networks favored the influence of most-recent pattern presentations.

One source of inspiration came from Fukushima's multi-layered neural network for visual (Japanese kanji) character recognition [17]. In this early work, Fukushima anticipated the now-common convolutional neural network. In Fukushima's approach, activated nodes in the intermediate layers could form lateral connections with each other; connections that were not possible with the discriminative (e.g., supervised learning for a Multilayer Perceptron) or the generative (e.g., stochastic resonance, which was the precursor for contrastive divergence in the Boltzmann machine, and later the restricted Boltzmann machine).

The work by Steve Grossberg and Ennio Mingolla in developing the Boundary Contour System (BCS), to emulate low-level mammalian visual processes, also influenced notions of how a CVM could play a role in a computational system [18, 19]. Grossberg and Mingolla used the gestalt laws of perceptual grouping to guide certain low-level visual processes, such as connecting short line segments if they occurred in the same line with each other and were sufficiently close to each other. This overcame significant difficulties in early computer vision systems. In particular, Grossberg and Mingolla emphasized how certain factors could cause connections between low-level processing units in a system. This would activate nodes that previously had not been active, to create at least contiguous line segments (if not clusters).

Thus, one of the key inspirations for using the CVM in a neural network-based computational system came not from the now-classic discriminative and generative architectures, but from researchers who considered how lateral connections between active nodes might be useful.

2.3 Potential role for a CVM system

Maren conceived the notion that if an entire CVM grid was used to create a set of responses to a given input stimulus, then the activation of certain nodes might decay gradually over time, and that lateral connections (created via Hebbian learning) between active nodes might stabilize responses to not only a currently-presented pattern, but also responses to short pattern sequences.

The unique insight that came from interactions with Pribram and colleagues was that a 1-D or 2-D CVM could model interacting domains

of neurons. As a step beyond the then-current thinking of neural networks as “neural modeling systems,” the CVM-based approach recognized the crucial role of creating clusters or physically-connected groups of neurons (neural domains) as the means by which neural systems responded to stimuli.

One component of this insight was the realization that neural networks had hidden (latent) node activations that occurred in isolation from each other; each activation was strictly in response to learned connection weights each modulating inputs from the stimulus patterns. This meant that a given node’s activation was dependent on the stimulus immediately feeding into it from the current pattern presentation. Even the backpropagation-through-time and recurrently-connected neural networks had sharp decays on the influence of prior patterns on a given node’s activation.

If a CVM approach were used, then a cluster of active nodes might potentially be more self-stabilizing than a single activated node. This self-stabilization could be enhanced by allowing lateral connections to form within an activated node cluster. Multiple factors could then impact how long the cluster’s activation would persist. In fact, a cluster of activated nodes could potentially degrade node-by-node, where the nodes in the cluster core maintained longer temporal activation. This would potentially compare favorably with the single-node activation methods of existing neural networks. It could also potentially make a cluster more robust against temporal perturbations.

The key was that free energy minimization, which was already used to guide connection weight development between network “layers,” could also be used *within* a given layer as a secondary process. This CVM-based within-layer free energy minimization would not only produce a stable (if redundant) set of responses to pattern stimulus, it could also be a stabilizing force against perturbations. CVM free energy minimization (together with adjustable slow decay of activated nodes) could also be used to help a network learn temporal pattern association.

With modest grant support from the Jeffries Foundation, Maren and colleagues developed an initial, 1-D proof-of-concept testbed for the CVM within a computational framework. Maren christened this the CORTECON, for *C*Ontent-*R*etentive, *T*Emporally *C*ONnected neural network. This led to three brief conference paper presentations between 1992 and 1994 [20, 21, 22].

For various reasons (mostly having to do with severe intellectual

property assignment agreements), the ideas behind the CORTECON languished from the mid-1990's until 2016, when Maren re-introduced this approach [23]. This work largely addressed the 1-D CVM, and did not include computational results for minimizing free energy across a 2-D CVM system.

Maren's 2016 work was presaged by a small set of privately-produced technical reports, reviewing the CVM theory and presenting detailed derivations that were not included in the original Kikuchi (1951) and Kikuchi and Brush (1964) papers. One of these works specifically addressed the 2-D CVM (Maren, 2014) [24].

2.4 Further role for the CVM

There is a philosophical connection between the notion of using a 2-D CVM to model a physical system and the ideas advanced by Karl Friston regarding the role of free energy minimization as a key function in brain processes (2010, 2013, 2015) [27, 28, 29].

Friston's equations extend the variational Bayes approximation (for example as explained by Beal (2003)[30]) into a framework in which an external system is represented by a system that is separated from the external system via a Markov blanket. The representational system is then modeled directly. Maren has produced a detailed description of the Friston's approach to using variational Bayes as compared with the classic approach [31].

One component of variational Bayes is that the modeling system should be brought as close as possible to the representational system. The notion of the variational Bayes approximation uses a formal resemblance between the approximation equations and statistical mechanics. Maren [31] suggested that the process of modeling need not be simply adjusting parameters to reduce a Kullbeck-Leibler divergence, but actually carrying out a real free energy minimization. For some systems, the 2-D CVM would be an appropriate means for conducting this real free energy minimization.

2.5 CVM applications summary and barriers to entry

For a method that was invented back in the 1950's, the CVM approach has been relatively under-utilized. The overwhelming applications

have been to the study of phase transitions and phase diagrams in 3-D systems.

While some leading researchers have identified the role of the CVM within the larger scope of graph theory and machine learning methods, it has not yet been practically applied to artificial intelligence or machine learning. In fact, there are no known instances of using a 2-D CVM to model any topographic system (other than the previously-cited work by Barton and Cocco [15]). This is surprising, considering that the CVM seems to be an ideal means for modeling 2-D topographies and even dynamics.

There are several difficulties that may have been barriers to entry. One is that Kikuchi and Brush (1967) presented the derivation of the analytic solution for the 2-D CVM configuration variables as a result, but without any of the intervening steps. The derivation of their result is a somewhat complex (and tedious and delicate) task. It has not previously been published in its entirety, except as a privately-published technical report by Maren (2014) [24].

Further, the code necessary to do even the most elementary CVM computations is likewise both substantive and delicate. Such code is not yet in the public domain, so that any researcher contemplating work in this area would be faced with extensive *ab initio* code development. (See note at the end of this document for information on this author's code release.)

This paper attempts to make the 2-D CVM approach more accessible to a diverse range of researchers. It presents, in Appendix A, the complete derivation of the configuration variables at equilibrium (for the singular case where such an analytic solution is possible, at $x_1 = x_2 = 0.5$). It also presents a baseline study of the thermodynamic properties of the 2-D CVM.

The cluster variation method uses a set of topographic variables, called the *configuration variables*, as identified in the following Table 2.

The following Section 3 discusses these configuration variables in depth.

3 The Configuration Variables

The key requirement to working with the cluster variation method is that we need to understand and use a set of *configuration variables*. In a simple Ising system (the simplest statistical mechanics model for

Table 2: Configuration Variables for the Cluster Variation Method

Name	Variable	Instances
Unit	x_i	2
Nearest-neighbor	y_i	3
Next-nearest-neighbor	w_i	3
Triplet	z_i	6

a system in which only two states are possible for each unit), we only need to think about whether a given unit is “on” or “off,” or in states **A** or **B**.

We really only need one variable to describe the distribution of units in the system, because if we let x_1 be the fraction of nodes in state **A**, and x_2 be the fraction of nodes in state **B**, then we also have that $x_2 = 1 - x_1$. This gives us a system that is relatively easy to model and visualize.

In contrast, in the CVM, we expand the set of variables under consideration. We use a set of variables that are collectively referred to as the *configuration variables*.

In this section, we address three key factors that are essential for working with the *configuration variables*:

1. ***Configuration variable definitions*** – how they show up in the 2-D CVM grid,
2. ***Counting the onfiguration variables*** – how each configuration variable is counted, and the V&V thereof (verification and validation), and
3. ***A brief interpretation*** – how to interpret configuration variable values.

Later in this paper, we will examine how configuration variables change with the enthalpy parameters. However, even before we connect the grid topographies (expressed via configuration variables) with the free energy equation, we can establish a foundation for understanding what the configuration variables mean (in practical terms), and how they interact with each other.

3.1 Introducing the Configuration Variables

A 2-D CVM is characterized by a set of *configuration variables*, which collectively represent single unit, pairwise combination, and triplet values. The configuration variables are denoted as:

- x_i - Single units,
- y_i - Nearest-neighbor pairs,
- w_i - Next-nearest-neighbor pairs, and
- z_i - Triplets.

These configuration variables are illustrated for a single zigzag chain in Figure 2.

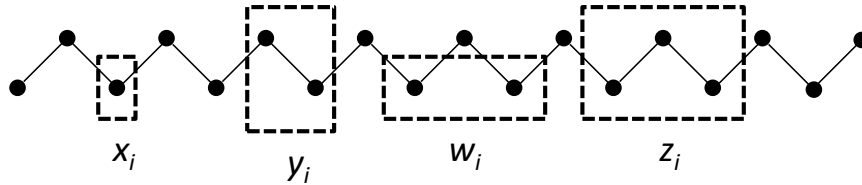


Figure 2: The 1-D single zigzag chain is created by arranging two staggered sets of M units each. The configuration variables shown are x_i (single units), y_i (nearest-neighbors), w_i (next-nearest-neighbors), and z_i (triplets).

For a bistate system (one in which the units can be in either state **A** or state **B**), there are six different ways in which the triplet configuration variables (z_i) can be constructed, as shown in Figure 3.

Notice that within Figure 3, the triplets z_2 and z_5 have two possible configurations each: **A-A-B** and **B-A-A** for z_2 , and **B-B-A** and **A-B-B** for z_5 . This means that *there is a degeneracy factor of 2* for each of the z_2 and z_5 triplets. This is shown in Figure 3 and also identified earlier in Table 2.

The degeneracy factors β_i and γ_i (number of ways of constructing a given configuration variable) are shown in Figure 4. For the pairwise combinations y_2 and w_2 , $\beta_2 = 2$, as y_2 and w_2 can each be constructed as either **A-B** or as **B-A** for y_2 , or as **B- -A** or as **A- -B** for w_2 . Similarly, $\gamma_2 = \gamma_5 = 2$ (for the triplets), as there are two ways each for constructing the triplets z_2 and z_5 . All other degeneracy factors are set to 1. See the illustrations in Figs. 3 and 4.

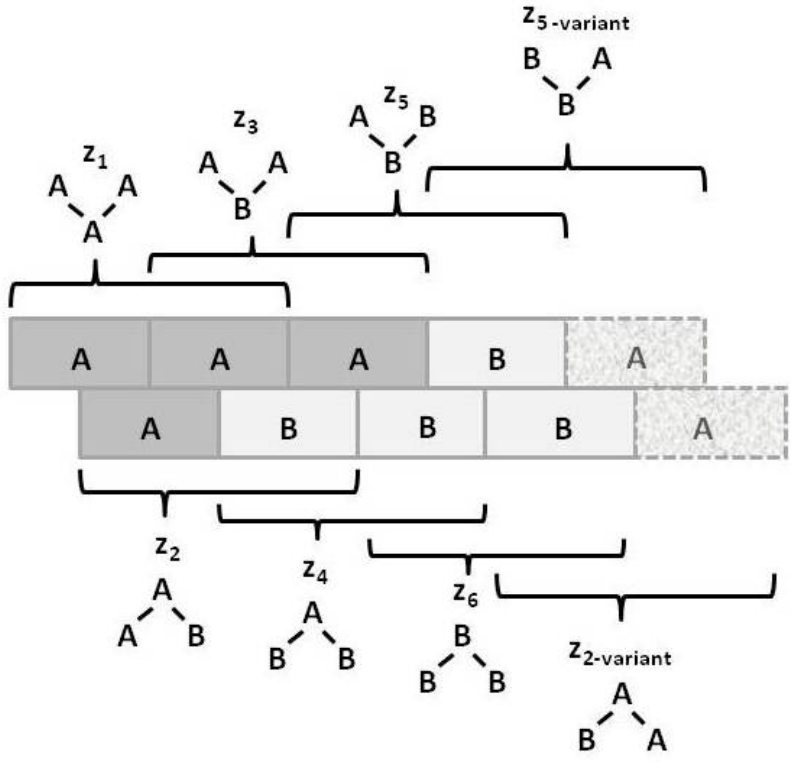


Figure 3: The six ways in which the configurations z_i can be constructed.

3.2 Counting the Configuration Variables

The first step in working with a 2-D CVM was to construct a computer program that would count the various neighboring pairs and triplets, and produce the resulting configuration variables. All computer code was devised in Python 3.6, using straightforward programming design. (The next major code iteration will require an object-oriented approach.)

One of the most important verification and validation (V&V) steps with these programs was to ensure that they accurately computed the various configuration variables, as described in Maren (2018) [25].

The early experiments with a 2-D CVM system (forming the bulk for the experimental work discussed here) were all done using various grids of 256 (16 x 16) units each. Two of these grids are illustrated in Figure 5.

The Unit Configurations			The Nearest Neighbor Configurations				The Next-Nearest Neighbor Configurations			
Pattern <i>(Unit)</i>	A	B	Pattern <i>(Nearest Neighbor)</i>	A-A	A-B B-A	B-B	Pattern <i>(Next-Nearest Neighbor)</i>	A--A	A--B B--A	B--B
Config. Variable	x_1	x_2	Config. Variable	y_1	y_2	y_3	Config. Variable	w_1	w_2	w_3
Degeneracy	1	1	Degeneracy	1	2	1	Degeneracy	1	2	1

The Triplet Configurations						
Pattern <i>(Triplet)</i>	A-A-A	A-A-B B-A-A	A-B-A	B-A-B	B-B-A A-B-B	B-B-B
Config. Variable	z_1	z_2	z_3	z_4	z_5	z_6
Degeneracy	1	2	1	1	2	1

Figure 4: Illustration of the *configuration variables* for the cluster variation method, showing the ways in which the configuration variables y_i , w_i , and z_i can be constructed, together with their degeneracy factors β_i and γ_i .

Keeping initial experiments confined to this relatively small 16x16 (256-unit) grid allowed three things:

1. **Sufficient variety in local patterns** – this grid size was large enough to illustrate several distinct kinds of topographies (each corresponding to different *h-values* or enthalpy parameters; *h-values* will be discussed in a following section),
2. **Sufficient nodes** – there were enough nodes so that triplet-configuration extrema could be explored in some detail (e.g., for relatively small numbers of nodes in state **A**, and
3. **Countability** – the V&V effort required that several early versions of the grid be *manually counted* for all the configuration values for a given 2-D grid configuration, and matched against the results from the program.

One final advantage of the 16 x 16 grid layout was that the different

grid configurations were both large enough to show diversity, but small enough so that it was possible to manually create figures illustrating the activation states (**A** or **B**) of each node, thus illustrating the detailed particulars of each configuration design. (The code at this point included only rudimentary print-outs of grid patterns.)

The experiments began with manually-designed grid configurations, such as the two shown in Figure 5. These two configurations correspond (somewhat) to the notions of “scale-free” and “rich club” topographies, as observed in various neural communities. (For references to the scale-free and rich club literature on brain topographies, please consult Maren (2016) [23].)

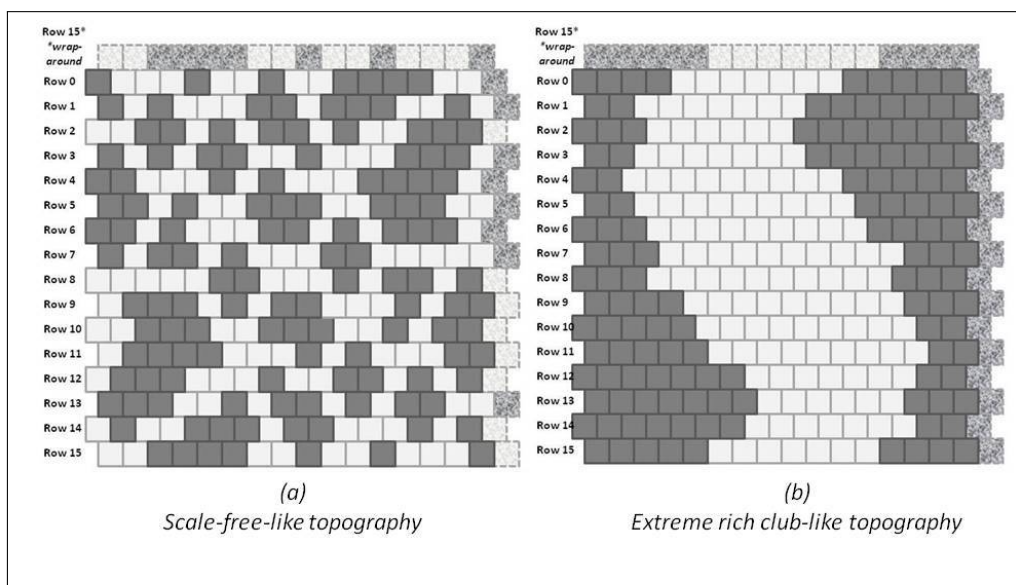


Figure 5: Illustration of the two different grids for experiments with the 2-D CVM system.

These two different grid configurations are early attempts to characterize how the h -values can be identified for grids with different total configuration variable values. The following sections will discuss h -values in the context of the free energy equation.

Both of these systems were created with the constraint of equiprobable occurrence of units in states (**A** or **B**; that is, $x_1 = x_2 = 0.5$). This was done to facilitate the necessary code V&V step, which will be

discussed in later in this section. Thus, for the configurations shown in Figure 5, both the *(a)* and *(b)* grids have 128 nodes each of units in state **A** and in state **B**.

The configuration on the left of Figure 5 is an effort to build a “scale-free-like” system. The notion of a “scale-free” system is that the same kind of pattern replicates itself throughout various scales of observation in a system. Thus, for the “scale-free-like” configuration shown in Figure 5 *(a)*, the design was originally intended to be 180-degree symmetrical around a central axis (dihedral group-2 symmetry). Specifically, the left and right sides were to be identical in a rotated-180-degree sense.

For ease in design of the “scale-free-like” system, there was a single larger pattern on one side and duplicated on the other. The basis for this pattern was a paisley-like shape of **A** units. This shape was designed in order to create greater dispersion of values across the z_i triplets; that is, to minimize having tightly-clustered islands that would yield little in the way of **A-B-A** and **B-A-B** triplets (z_2 and z_5 , respectively).

The practical limitation of attempting to fit various “islands” of **A** nodes (black) into a surrounding “sea” of **B** nodes (white) meant that there were not quite enough **B** nodes to act as borders around the more compact sets of **A** nodes. Thus, the pattern in the right half of grid *(a)* is a bit more compressed than originally planned.

The original plan was that out of 256 nodes in the grid, half (of the designed pattern) would be on the right, and half on the left; 128 nodes on each side. Of these, for each side, 64 nodes were to be in state **A** (black). Of these nodes (per side), sixteen (16 nodes) would be used to create a large, paisley-shaped island. The remaining $64 - 16 = 48$ nodes would be used for smaller-sized islands; two islands of eight nodes each, etc. The plan is shown in Figure 6. The notation of “center” and “off-center” refers to the placement of the various islands; the largest (16-node) islands were to be placed more-or-less in the center of each of their respective (left or right) sides of the grid, and the remaining islands were to be “off-center”; situated around their primary respective large islands.

The resulting patterns (shown in Figure 6) were close to the original plan, although not exactly the same.

Even though some changes had to be made to the original design plan, the original constraint, that the number of units in states **A** and

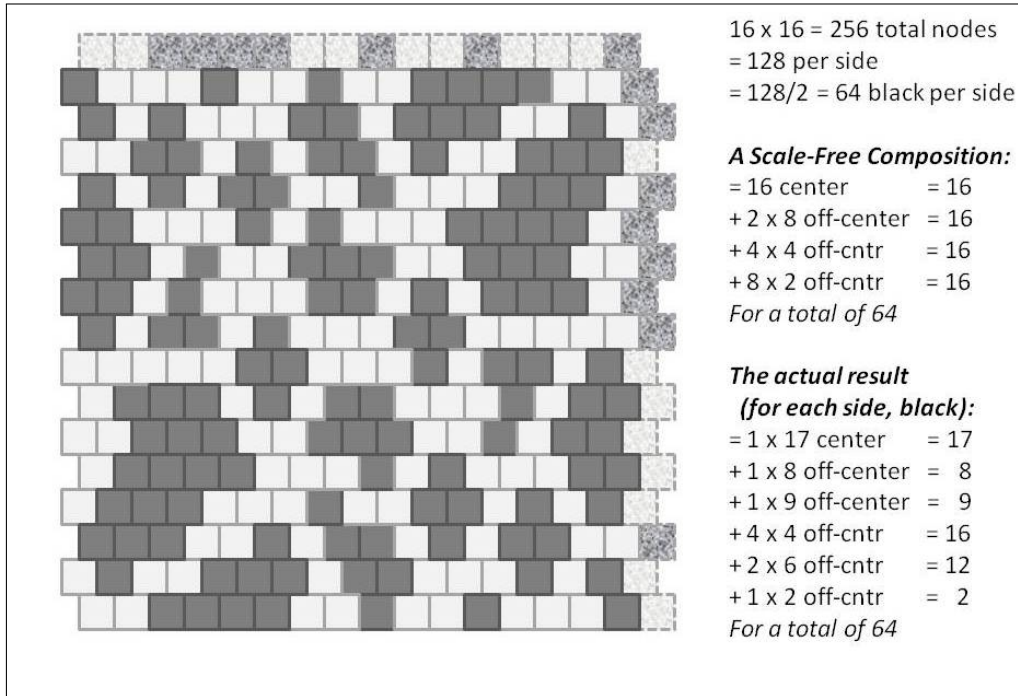


Figure 6: A 2-D CVM “scale-free-like” system with an equal number state **A** and state **B** nodes (128 nodes each).

B would be identical (128 nodes in each), was kept. The details are shown in Figure 6.

The validation step for this stage of code development was to manually count all the configuration variables for several different configuration grids, such as the ones shown in Figure 5.

The counts for the “scale-free-like” grid shown in Figure 6 are shown in Figure 7. It suffices to say that the results from the manual counting (of all configuration variables) and those created by the computer code were identical. These held true across several different grids with different node configurations.

Note: To achieve the fractional variables shown in Figure 3, and also in Table 2, the following relations are used:

- $x_i = X_i$,
- $y_i = Y_i/2$, for $i = 1, 3$ and $y_2 = Y_2/4$, accounting for the degeneracy with which y_2 occurs,

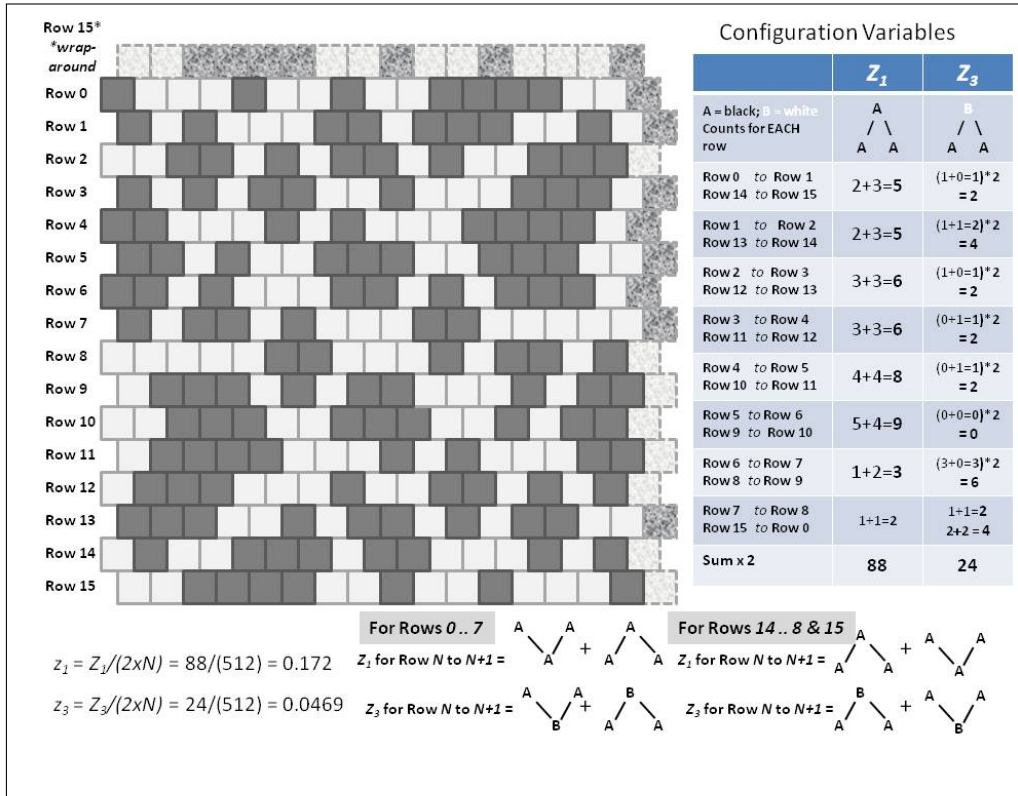


Figure 7: A 2-D CVM “scale-free-like” system with an equal number state **A** and state **B** nodes (128 nodes each).

- $w_i = W_i/2$, for $i = 1, 3$ and $w_2 = W_2/4$, accounting for the degeneracy with which w_2 occurs, and
- $z_i = Z_i/2$, for $i = 1, 3, 4, 6$ and $z_2 = Z_2/4$, $z_5 = Z_5/4$, accounting for the degeneracy with which z_2 and z_5 occur.

Note: The exact details of the row counts are difficult to read in Figures 7 and 8; the original diagrams are in a corresponding slidedeck that is available in the associated GitHub repository [26].

Note: The count for the z_i variables is approximate; not exact. A follow-on code analysis revealed that while the counting steps for the x_i , y_i , and w_i configuration variables was precise, the counting for the z_i configuration variables was done only across the horizontally-expressed variables, and did not include the vertical versions. This was true for both the computer code and the manual counting. Because the size

and diversity of patterns within any of the testing grids was sufficient to give a reasonably accurate result for the z_i , the code was kept as-is. The decision to use the approximate values for the z_i was supported via manual counts on some very small-scale 2-D grids. Another reason to stay with the current code (for approximate results) is that the next step will be a transition to a full object-oriented approach, and the time spent on code revision would be best served by moving on to the next stage.

The second configuration, for an “extreme-rich-club-like” configuration, is shown in Figure 8.

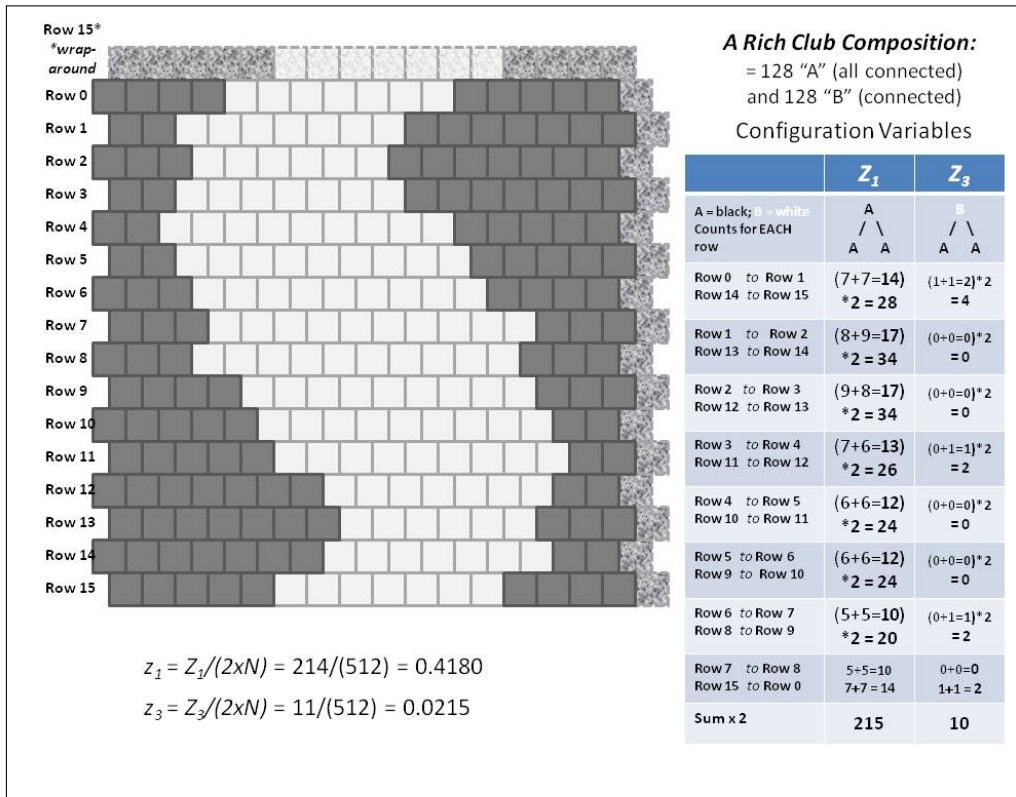


Figure 8: A 2-D CVM “extreme-rich-club-like” system with an equal number state **A** and state **B** nodes (128 nodes each).

As a contrast to the “scale-free-like” grid configuration used in Figures 6 and 7, the contrasting experiment used a second configuration

that had only one large compact region of nodes in state **A**, which was wrapped-around the grid envelope, as shown in Figure 8. This configuration was designed to maximize the number of pairwise and triplet configurations that put “like-near-like.” The previous configuration, shown in Figure 6, was more in the direction of “like-near-unlike.”

The purpose of having patterns with such different dispersions among the configuration variable values was that they would putatively correspond to different h -values. This means that they would (ultimately) converge to different points on an equilibrium curve for the free energy equation (in the case of equiprobable units in states **A** and **B**).

We have the analytic results for the free energy minimum curve; specifically the equilibrium point for the free energy at different h -values, or interaction enthalpy values. (The details for the free energy will be presented in the next section.) Thus, knowing what the anticipated h -value would be for a given pattern, it would be interesting to find the *actual* set of configuration variable values that result when the initial 2-D CVM grid is brought to free energy equilibrium, for the identified *target h-value*.

These experiments would also serve the verification and validation (V & V) process in vetting the code. See Maren (2018) [25] for the V & V Technical Report, and Maren (2019) for a slidedeck (available on GitHub) capturing details of the experimental results [26].

By far, the most complex element of the “configuration variable counting” code was in counting the triplets. The V&V step ensured that the counts wrapping around from right to left, and from top to bottom (creating a completely-wrapped envelope of the initial 2-D grid) performed as desired and expected. (See the *Note* earlier in this section; the counts for the z_i variables are done in the horizontal direction only, for both the code and manual verification.)

4 Topographies: Interpreting configuration variables

When we work with a typical Ising system model, we can easily interpret the results in terms of simple dependence of various functions on a single variable, x_1 . The topographic organization of the system, in this simple case, is not important.

In contrast, when we work with a 2-D CVM, *the topographic*

organization is all-important. Further, we have fourteen different configuration variables that collectively describe this topography. This collection of variable values is a bit too much to keep in mind!

Thus, we need some guidelines for interpreting the system, given the set of configuration variables that are achieved at a free energy equilibrium point. Also, we need to reduce the number of variables that we think about to an absolute minimum, so that we can mentally capture the essentials of a given free energy solution.

Also, we need to be able to mentally correlate this very small set of “think-worthy” configuration variables with some notion of what the topography would be like. We understand, of course, that we won’t be envisioning a *specific* topology; rather, we would be envisioning a *kind of* topology.

What we will move towards is a reduced set of just *three configuration variables* that we need to consider, if we want a fairly good mental approximation of the 2-D CVM grid topography.

With this in mind, we break this process down to two manageable steps:

1. *Reduce the number of “think-worthy” configuration variables* to an absolute minimum, and
2. *Interpret the meaning* of each of these few configuration variables.

As noted above, there are a total of fourteen different configuration variables; two x_i , three each for the y_i and w_i , and six of the z_i .

Fortunately, we don’t need to think about all fourteen configuration variables. In fact, we can get a very good sense of the 2-D CVM grid composition by just considering three configuration variables; z_1 , z_3 , and y_2 . These are selected because, taken together, they are reasonably descriptive of the grid topography:

- z_1 - **A-A-A** triplets; indicates the relative fraction of **A** units that are included in “islands” or “land masses”; this also (indirectly) indicates the compactness of these masses,
- z_3 - **A-B-A** triplets; indicates the relative fraction of **A** units that are involved in a “jagged” border (one that involves irregular protrusions of **A** into a **B** space), or the presence of one or more “rivers” of **B** units extending into landmass(es) of **A** units, and
- y_2 - **A-B** nearest-neighbor pairs; indicates the relative extent to which the **A** units are distributed among the surrounding **B**

units. A higher y_2 value indicates lots of boundary areas between **A** and **B**, and a smaller value indicates large “landmasses“ of **A** units.

4.1 First simplification: consider the equiprobable case

We can greatly simplify the complexity of our task by dealing with the *equiprobable distribution* case, where $x_1 = x_2 = 0.5$. We are doing this, not only because it makes it easier to think about the system, but because at this equiprobable distribution point, *we can achieve an analytic solution for the configuration variables*.

Further, at this equiprobable distribution point, we can also *invoke certain equalities among the configuration variables, due to symmetry considerations*. Thus, at this point, we would have:

- $x_1 = x_2$ - units in state **A** equal those in state **B**,
- $y_1 = y_3$ - nearest-neighbor pairs **A-A** equal **B-B**,
- $w_1 = w_3$ - next-nearest-neighbor pairs **A- -A** equal **B- -B**,
- $z_1 = z_6$ - triplets **A-A-A** equal **B-B-B**,
- $z_2 = z_5$ - triplets **A-B-A** equal **B-A-B**, and
- $z_3 = z_4$ - triplets **A-A-B** equal **A-B-B**.

Thus, if we have the values for x_1, y_1, w_1, z_1, z_2 , and z_3 , then we also have the values for x_2, y_3, w_3, z_6, z_5 , and z_4 .

Further, our normalization constraints also mean that if we know y_1 (and thus also y_3), we also know y_2 , because we have $y_2 = 0.5(1.0 - y_1 - y_3)$. Similarly, we also would have w_2 .

Also, we can rewrite these expressions; if we have y_2 , then we have $y_1 = y_3 = 0.5 - y_2$, and similarly for w_1 and w_3 if we have w_2 .

4.2 Simplifying the numbers of z_i

Similarly, we have the normalization for the z_i configuration variables given as

$$1 = x_1 + x_2 = \sum_{i=1}^6 \gamma_i z_i. \quad (1)$$

Thus, in the equiprobable case, we have

$$0.5 = \sum_{i=1}^3 \gamma_i z_i = z_1 + 2z_2 + z_3. \quad (2)$$

Thus, if we know z_1 and z_3 , we also know z_2 , given as $z_2 = 0.25 - (z_1 + z_3)/2$.

In short, at the equiprobable distribution point (where $x_1 = 0.5$), if we know y_1 , w_1 , z_1 , and z_3 , then we also know the remaining configuration variables.

4.3 Relationship between y_i and w_i

As one more step, we will note that, most of the time, y_i and the corresponding w_i will be approximately close to each other. In particular, the nearest-neighbor configuration variable y_2 indicates the extent of like-near-unlike boundaries. In the very extreme case where the units are arranged in a “checkerboard”-like configuration, then y_2 will approach its maximum of 0.5 (and $2y_2 \rightarrow 1.0$), while the values for y_1 and y_3 , indicating like-near-like nearest neighbors, will both approach 0.

(As a side note, it is worthwhile to make sure that we don’t push the system so far that either y_1 or y_3 approaches 0, as the entropy term involves multiple instances of computing $v \ln(v) - v$, where v refers to a configuration variable, and we don’t want to go to the extreme of taking the logarithm of 0.)

At the other extreme, a very small value for y_2 indicates that the system is composed almost exclusively of a very large mass of **A** units, existing as a single “continent” in a sea of **B** units. There is no single minimum value for y_2 , as it really becomes a function of the overall number of units in the system; as we create a progressively larger and larger grid, the fraction of units on the boundary of a large **A** continent becomes smaller in comparison to the total number of units actually in the interior of this large mass (with progressively more **A-A** nearest neighbors).

The w_i values, representing next-nearest-neighbor pairs, will not exactly be the same as the y_i . However, in the case of having large

“landmasses“ of **A** in a sea of **B**, then (similar to the y_1 and y_3), the values for w_1 and w_3 will each approach their limits of 0.5, and the value for w_2 will shrink (getting close to but not reaching 0).

As visual interpretations, we can think that y_2 reflects the relative proportion of like-near-unlike boundary pairs across the diagonals, and w_2 reflects the like-near-unlike boundary pairs along the horizontal and vertical connections. Thus, in Figure 8 (with a large landmass of **A** units, wrapped around from right-to-left, so it appears as two distinct halves in the figure), we have relatively small values for both y_2 and w_2 .

In contrast, in the earlier Figure 6, we have lots of small ‘islands’ of **A** units scattered throughout the sea of **B**; both y_2 and w_2 are substantively increased.

Similar to y_1 , z_1 indicates the extent of large, contiguous “landmasses“ of **A** units. In particular, it indicates the *compactness* of these landmasses.

The z_3 value reflects less the presence of a boundary between masses of **A** and **B** units, and more the complexity of the boundary. The z_3 value also increases when we have long, spider-leg-like connections between masses or islands of **A** units. (Similarly, the value for z_4 increases when we have “rivers“ of **B** appearing within the **A** landmasses.)

4.4 Single starting point, two resulting topographies

Although we will have a more detailed description later, we will get a better understanding of the relationships among the various configuration variables by introducing two comparative examples here. This work was done as Trial 2 during the experimental process.

We begin with the scale-free-like initial grid, introduced earlier in Figure 6. We will bring this initial grid to a free energy minimum point, for each of two different *h-values*:

- Trial 2.a: $h = 1.65$, which should push the system towards increased like-near-like clustering, and
- Trial 2.b: $h = 1.16$, which should push the system towards like-near-unlike pairs.

Trial 2.a

When we bring the system from Figure 6 to free energy equilibrium with $h = 1.65$, we get the result shown in Figure 9.

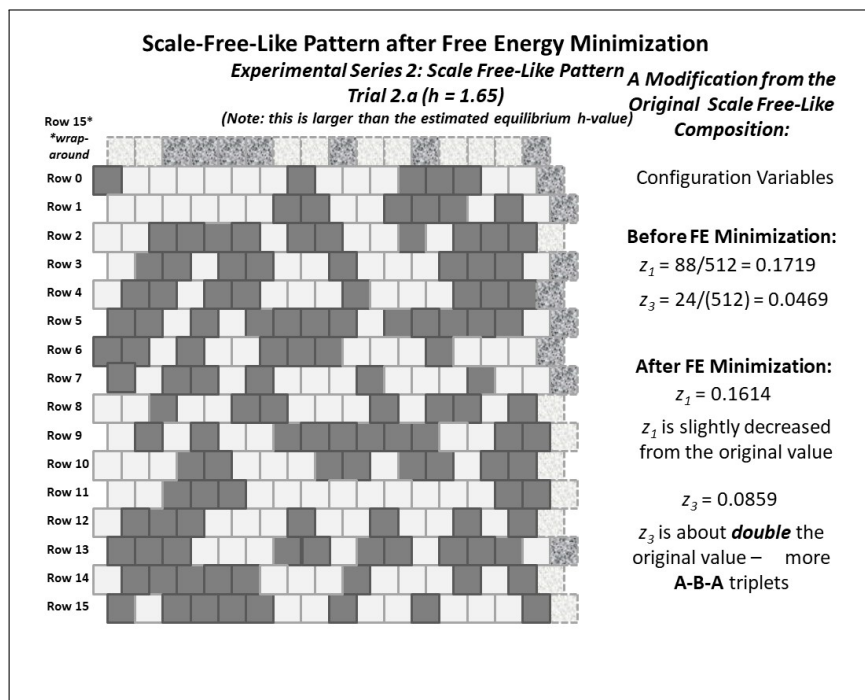


Figure 9: A 2-D CVM “scale-free-like” system, originally presented in Figure 6, brought to a free energy minimum with $h = 1.65$.

We see in Figure 9 that, as expected, the clusters are coalesced as compared with the original pattern.

Trial 2.b

When we bring the system from Figure 6 to free energy equilibrium with $h = 1.16$, we get the result shown in Figure 10.

With a lower h -value than was previously used, we expect less clustering of like-with-like, and more spread-out connections. What we see is interesting - not surprising - but it is worth noting that we get a number of “spider-leg” connections between what remains from the original clusters.

These “spider-legs” give us *both* like-near-like (extending the length of the spider-leg) as well as like-near-unlike (on either side of the spider-leg) connections for each unit in the leg. Thus, each unit in a spider-leg gives us approximately the ratio of y_1 and y_2 pairwise

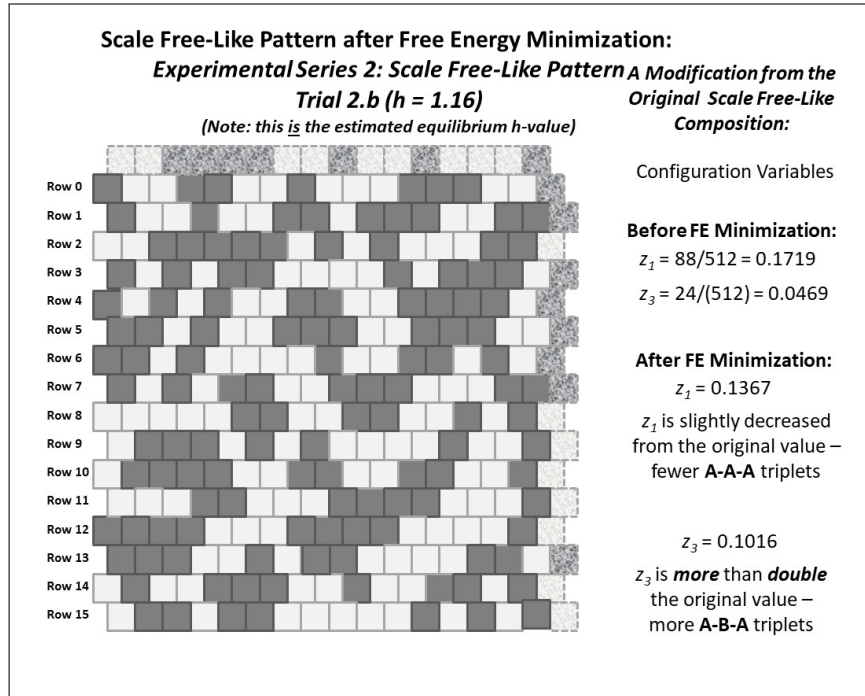


Figure 10: A 2-D CVM “scale-free-like” system, originally presented in Figure 6, brought to a free energy minimum with $h = 1.16$.

connections (two y_2 connections per y_1 , accounting for the factor of two degeneracy in the y_2 pairs) that we’d expect near $h = 1.0$.

5 The 2-D CVM Free Energy

The essential notion of the CVM is that we work with a more complex expression for the free energy in a system.

As a point of comparison, the basic Ising equation is

$$\bar{F} = F/(Nk_{\beta}T) = \bar{H} - \bar{S}, \quad (3)$$

where F is the free energy, H is the enthalpy and S is the entropy for the system, and where N is the total number of units in the system, k_{β} is Boltzmann’s constant, and T is the temperature.

For working with abstract systems, the total $Nk_{\beta}T$ can be absorbed into a *reduced energy formalism*, as these values are constants during

system operations. This leads to the *reduced representations* of \bar{F} , \bar{H} , and \bar{S} . We will work consistently with reduced representations throughout this work.

In a simple Ising model, both the enthalpy H and the entropy S can be computed based on only the relative fraction of active units in a bistate system. That is, there are only two kinds of computational units; *active* ones in state **A**, where the fraction of these units is denoted x_1 , and *inactive* ones in state **B**, where the fraction of these units is denoted x_2 . (Of course, $x_1 + x_2 = 1.0$.)

In contrast to the simple entropy used in the basic Ising model in statistical mechanics, in the CVM approach, we expand the entropy term. The CVM entropy term considers not only the relative fractions of units in states **A** and **B**, but also that associated with the *configuration variables*, as described earlier in Section 3.)

We can write the 2-D CVM free energy, using the formalism first introduced by Kikuchi in 1951 [1], and then further advanced by Kikuchi and Brush (1967) [2] (explicitly for the 2-D CVM), as

$$\begin{aligned} \bar{F}_{2-D} = F_{2-D}/N = & \\ & \bar{H}_{2-D} - \bar{S}_{2-D} \\ & + \mu \left(1 - \sum_{i=1}^6 \gamma_i z_i \right) + 4\lambda (z_3 + z_5 - z_2 - z_4), \end{aligned} \tag{4}$$

where μ and λ are Lagrange multipliers, and we have set $k_\beta T = 1$.

5.1 The 2-D CVM Enthalpy

The enthalpy in a simple Ising system is traditionally given as

$$\begin{aligned} \bar{H}_{2-D} = H_{2-D}/N & \\ & = \bar{H}_0 + \bar{H}_1 \\ & = \varepsilon_0 x_1 + c x_1^2, \end{aligned} \tag{5}$$

where H_0 and c are constants.

The first term on the RHS (Right-Hand-Side) corresponds to the *activation enthalpy*, or enthalpy associated with each active unit. The second term on the RHS corresponds to the *interaction enthalpy*, or energy associated with pairwise interactions between active units.

In contrast, the enthalpy for the 2-D CVM is given as

$$\begin{aligned}
\bar{H}_{2-D} &= H_{2-D}/N \\
&= \bar{H}_0 + \bar{H}_1 \\
&= \varepsilon_0 x_1 + \varepsilon_1(-z_1 + z_3 + z_4 - z_6)
\end{aligned}
\tag{6}$$

Note that in the original work by Kikuchi and Brush, Eqn. 6 is simplified (K&B Eqns. I.16 and I.17) to

$$\bar{H}_{2-D} = \varepsilon_1(-z_1 + z_3 + z_4 - z_6), \tag{7}$$

that is, they omit the term linear in x_1 ; the activation enthalpy.

We can infer that Kikuchi and Brush omit the activation enthalpy from their enthalpy term because they move directly to the analytic solution for the 2-D CVM free energy, which is solvable only in the equiprobable distribution case of $x_1 = x_2 = 0.5$. The equiprobable distribution is achieved only when the activation enthalpy is zero; that is, when $\varepsilon_0 = 0$.

When the activation enthalpy $\varepsilon_0 > 0$, then the units in state **A** have an energy associated with them that is greater than that of the units in state **B**. Thus, an equilibrium solution will favor having fewer units in state **A**. There is no analytic solution for this case, other than that in which the interaction enthalpy is zero ($\varepsilon_1 = 0$). This latter case is trivial to solve, and is not particularly interesting, as the distribution of different kinds of nearest-neighbor pairs and triplets will be probabilistically random, excepting only that the proportions of units in states **A** and **B**, respectively, will be skewed by the activation enthalpy parameter ε_0 .

As just noted, the typical expression for the interaction enthalpy is a quadratic term in x_1 , that is, $H_1 = cx_1^2$. The parameter c encompasses both the actual interaction energy for each pairwise interaction, and a constant that expresses the distribution of pairwise interactions as a simple linear function of the fraction of active units (x_1) surrounding a given active unit. This is then multiplied by the total fraction of active units, giving the quadratic expression.

In the expression for the 2-D CVM interaction enthalpy, we have terms that expressly identifies the total fraction of nearest-neighbor “unlike” pairs (y_2) and “like” pairs (y_1 and y_3). Thus, we can replace cx_1^2 with the fraction of “unlike” pairs (counted twice, to account for the degeneracy in how these pairs can be counted), and the fractions of “like” nearest neighbor pairs.

We recognize that this is a simplification; we are not counting interaction energies due to next-nearest neighbor pairs, the w_i , nor from the triplets z_i . We are, effectively, subsuming these into the pairwise interactions that are being modeled with the y_i .

We take the interaction enthalpy parameter ε_1 to be a positive constant.

We envision a system in which the free energy is reduced by creating nearest-neighbors of like units, that is, **A-A** or **B-B** pairs. (Decreasing the interaction enthalpy leads to decreasing the free energy, which is desired as we go to a free energy minimum, or equilibrium state.) Similarly, the interaction enthalpy should increase with unlike pairs, or **A-B** pairs (or vice versa).

Thus, we write the interaction enthalpy equation, following the formalism introduced by Kikuchi and Brush, as

$$\bar{H}_{2-D} = H_{2-D}/N = \varepsilon_1(2y_2 - y_1 - y_3). \quad (8)$$

We interpret this equation by noting that as we increase the fraction of unlike unit pairings (**A-B** or **B-A** pairs), we raise the interaction enthalpy. At the same time, if we're increasing *unlike* unit pairings, we are also decreasing *like* unit pairings (**A-A** and **B-B**), so that we are again increasing the overall interaction energy. (Note that the *like* unit pairings show up in Eqn. 8 with a negative sign in front of them.)

Thus, if we create a 2-D CVM that is like a checkerboard grid (alternating unit types), then we are moving to a higher interaction enthalpy and higher free energy, and away from a free energy minimum. If we create a grid such as that shown in the RHS of Figure 5, with all of the units in each state grouped together, respectively, then we lower the interaction enthalpy and correspondingly lower the free energy.

Clearly, if the interaction enthalpy were all that mattered, we would have a 2-D CVM grid like the one on the right in Figure 5. What keeps this from happening is the entropy term, which demands some distribution over different possible configurations.

Before moving on to the entropy, we note that we can express the interaction enthalpy using the triplet configuration variables z_i , instead of the nearest-neighbor pair variables y_i . We can do this by drawing on *equivalence relations* between the y_i and z_i variables. Those for y_2 are given as

$$y_2 = z_2 + z_4 = z_3 + z_5 \quad (9)$$

$$2y_2 = z_2 + z_4 + z_3 + z_5. \quad (10)$$

Notice that we have two ways of expressing y_2 in terms of the z_i , as shown in Eqn. ???. Since we want to work with the total $2y_2$, it is easy to express that as the sum of the two different equivalence expressions. This will prove useful later, when we analytically solve for the free energy minimum, or equilibrium point.

We also have equivalence relations for y_1 and y_3 , given as

$$y_1 = z_1 + z_2 \quad (11)$$

and

$$y_3 = z_5 + z_6. \quad (12)$$

This lets us write

$$\bar{H}_{2-D} = \varepsilon_1(2y_2 - y_1 - y_3) = \varepsilon_1(z_4 + z_3 - z_1 - z_6). \quad (13)$$

As a minor note, the enthalpy used in previous related work by Maren [24, 23], was

$$\bar{H}_{2-D} = H_{2-D}/N = \varepsilon_1(2y_2) = \varepsilon_1(z_2 + z_3 + z_4 + z_5). \quad (14)$$

The results given here are similar in form to the results presented in the two previous works by Maren; they differ in the scaling of the interaction enthalpy term.

5.2 The 2-D CVM Entropy

The entropy for the 2-D CVM is given as

$$\begin{aligned} \bar{S}_{2-D} = S_{2-D}/N = & \\ & 2 \sum_{i=1}^3 \beta_i Lf(y_i) + \sum_{i=1}^3 \beta_i Lf(w_i) \\ & - \sum_{i=1}^2 \beta_i Lf(x_i) - 2 \sum_{i=1}^6 \gamma_i Lf(z_i), \end{aligned} \quad (15)$$

where $Lf(v) = v \ln(v) - v$.

There were two primary means for obtaining validation that the code computing the thermodynamic variables was correct:

1. **Comparison with analytic for the equiprobable case** – for the case equiprobable distribution among the x_i variables ($x_1 = x_2 = 0.5$), I have developed an analytic solution, which gives a means for comparing the code-generated results against the expected (analytic) results, and
2. **Comparison with analytic for the case where the interaction enthalpy is zero** – the second means to check the code-generated results is for the case where the distribution of x values is not equiprobable, however the interaction enthalpy is set to zero ($h = 1$), and thus the exact distribution of other configuration values can be precisely computed, allowing further for exact analytic computation of thermodynamic variables.

5.3 Free Energy Analytic Solution

Kikuchi and Brush (1967) [2] provided the results of an analytic solution for the 2-D CVM free energy, for the specific case where $x_1 = x_2 = 0.5$. Specifically, making certain assumptions about the Lagrange multipliers shown in Eqn. 4, we can then express each of the configuration variables in terms of ε_1 .

More usefully, since the expression actually involves the term $\exp(2\varepsilon_1)$, and not ε_1 itself, it is much easier to use the substitution variable $h = \exp(2\varepsilon_1)$. We refer to h (or sometimes, the *h-value*), as the *interaction enthalpy parameter* throughout.

The full derivation of the set of equations giving the configuration variable values at equilibrium (i.e., at $x_1 = x_2 = 0.5$) is given in Appendix A.

The full set of these analytic expressions for the various configuration variables is couched in terms of a denominator involving h , specifically

$$\Delta = -h^2 + 6h - 1, \tag{16}$$

which Kikuchi and Brush present as their Eqn. (I.24) [2].

We recall that at the equiprobable distribution point, where $x_1 = x_2$, we have a number of other equivalence relations, e.g. $z_1 = z_6$, etc.

We then (following Kikuchi and Brush, in their Eqn. (I.25)) identify each of the remaining configuration variables as

$$\begin{aligned}
y_1 = y_3 &= \frac{(3h-1)}{2\Delta} \\
y_2 &= \frac{h(-h+3)}{2\Delta} \\
w_1 = w_3 &= \frac{(h+1)^2}{4\Delta} \\
w_2 &= \frac{(3h-1)(-h+3)}{4\Delta} \\
z_1 = z_6 &= \frac{(3h-1)(h+1)}{8\Delta} \\
z_2 = z_5 &= \frac{(3h-1)(-h+3)}{8\Delta} \\
z_3 = z_4 &= \frac{(-h+3)(h+1)}{8\Delta}
\end{aligned} \tag{17}$$

5.4 Divergence in the analytic solution

As is obvious from Eqn. 16, there will be a divergence in the analytic solution for the configuration variables at the free energy minimum, because the analytic solution contains a denominator term that is quadratic in h . Specifically, the term diverges for $h = 0.172$ or $h = 5.828$.

We are interested in the latter case, where the value of $h > 1$ indicates that $\varepsilon_1 > 0$, which is the case where the interaction enthalpy favors like-near-like interactions, or some degree of gathering of similar units into clusters. This means that we expect that the computational results would differ from the analytic as $h \rightarrow 5.828$. (Actually, the computational results diverge from the analytic substantially before this point.)

This would possibly have some impact, but we find that the real point of interest comes from examining the impact of higher h -values on the free energy itself. Increasing h increases the overall value of the enthalpy term, and makes it overwhelmingly dominant with regard to the entropy term.

5.5 Significance of h in the free energy

Because it is the *minimum in the negative entropy* that creates the possibility for minimizing the free energy, we need to have the entropy term play a role that is at least on par with the enthalpy. If the enthalpy term is overall too large, then there will be an adverse effect on finding a useful free energy minimum.

The impact of the *interaction enthalpy parameter* h on the overall free energy is shown in Figure 11, which presents the results when

$x_1 = 0.5$, which is the case where all of the results should conform with the analytic solution.

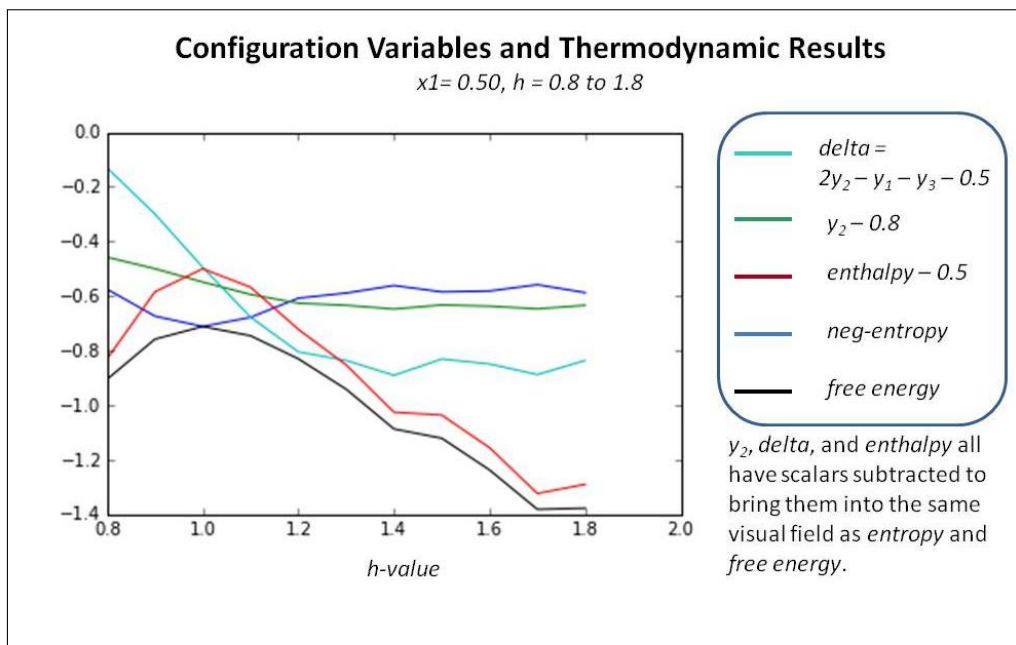


Figure 11: Configuration variable and thermodynamic values for the case where $x_1 = x_2 = 0.5$, and where the interaction enthalpy parameter h ranges as $h = 0.8..1.8$. See detailed explanation of results in the following Section 6, as their nature is similar to these results. Appendix D also contains detailed material relating to this figure.

We will discuss the results shown in Figure 11 in more detail in Section 7. First, we will put our attention on how, in general, we expect the h -values to influence the configuration variable results. We will do this in Section 6.

Before moving on, we briefly address the process for obtaining configuration variable values when we move away from the equiprobable case, which has been our mainstay up until now.

5.6 Moving away from the equiprobable case

As we just saw in Subsection 5.4, the analytic solution does not always hold. In fact, it has a divergence for a large value of the interaction en-

thalpy parameter. However, especially for low values of the interaction enthalpy, the analytic solution is a trustworthy starting place.

When we move away from the equiprobable case, we need a mechanism by which the pattern of node activations on the grid can adjust in order to reach a free energy minimum.

The code for accomplishing this works in two stages:

1. *Bring x_1 close to desired value*, and
2. *Adjust configuration variables to achieve free energy minimum.*

Early work on obtaining a more complete set of configuration variable and thermodynamic values was done as part of a set of *perturbation experiments*. That is, in addition to bringing a system to an initial free energy minimum point, the system was then “perturbed”. A fraction of the nodes were randomly selected for state-switching (from **A** to **B** and vice versa, keeping the relative proportions of nodes in each state the same). Then, the system was brought to a free energy minimum a second time. Visual inspection of the free energy graphs over time confirmed that the system tended to converge to approximately the same free energy minimum values.

The V&V aspects of this work are summarized in the V&V Technical Report; Maren (2018) [25]. Appendix D presents detailed material results.

The actual protocol by which an initial grid is brought to a free energy minimum (equilibrium state) will be discussed in the Technical Report that will immediately follow this one; it will similarly be published to arXiv. This *Protocol* document will provide detailed instructions and walk-throughs for working with a system designed to be at the equiprobable distribution point; that is, $\varepsilon_0 = 0$, but with interaction enthalpies conducive to forming like-near-like clusters; that is, $\varepsilon_1 = 0$.

6 Dependence of the configuration variables on the enthalpy parameters

From the analytic solution for the 2-D CVM, we can identify the configuration variables for a given *h-value*. The dependence of y_2 , z_1 , and z_3 on h is shown in the following Figure 12.

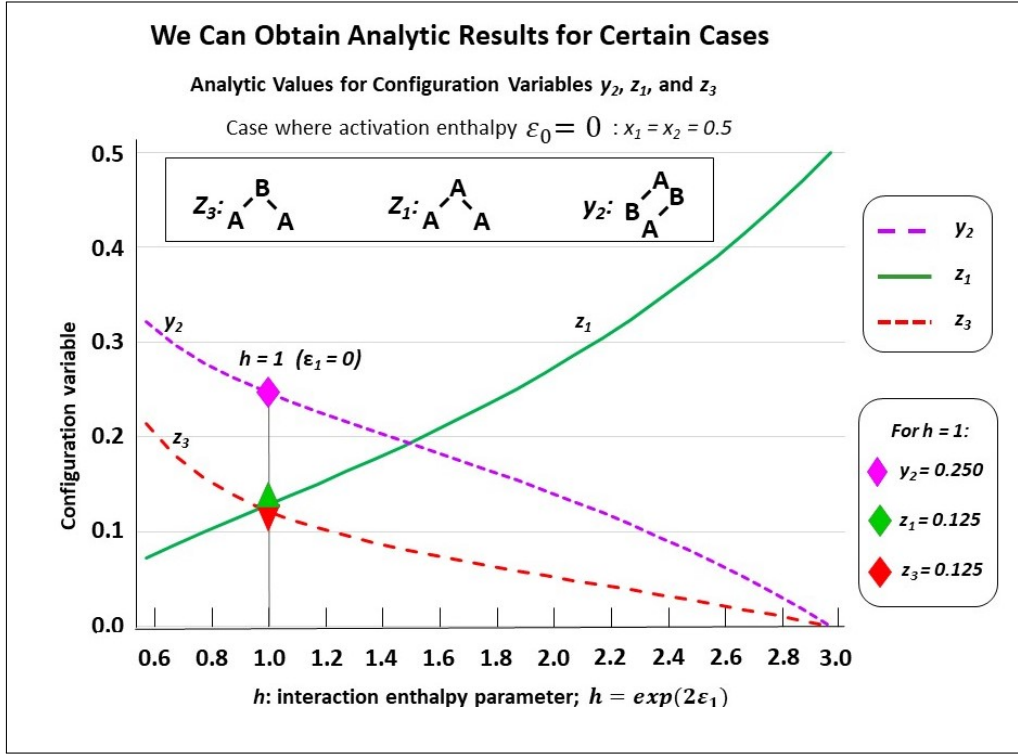


Figure 12: Dependence of the configuration variables y_2 , z_1 , and z_3 on the enthalpy parameter h , where $h = \exp(2\varepsilon_1)$.

The following three subsections assist in interpreting the results shown in Figure 12; these are the cases where the interaction enthalpy is defined as:

1. $\varepsilon_1 = 0$ so that $h = e^{2\varepsilon_1} = 1$,
2. $\varepsilon_1 < 0$ so that $h = e^{2\varepsilon_1} < 1$, and
3. $\varepsilon_1 > 0$ so that $h = e^{2\varepsilon_1} > 1$.

The material in these next three subsections was first in Maren (2016) [23], describing the dependence of configuration variables on h in a 1-D CVM system. The same essential arguments hold equally well for the 2-D CVM system, and are presented again here (with minor revisions) for completeness.

6.1 Configuration variables when the interaction enthalpy $\varepsilon_1 = 0$ ($h = 1$)

We begin by noting (in the slightly left-of-center portion of Figure 12, where $h = 1$) that the observed configuration variable values are exactly as we would expect. Specifically, $z_1 = z_3 = 0.125$, and $y_2 = 0.250$. This fits precisely with our expectation for the configuration variables at equilibrium when $\varepsilon_1 = 0$ ($h = e^{2\varepsilon_1} = 1$).

To understand intuitively that this would be the expected result, we reflect on the total number of triplet states available, together with their degeneracies. We use various normalization equations from Appendix A as well, and particularly note that

$$1 = x_1 + x_2 = \sum_{i=1}^6 \gamma_i z_i$$

Since we also have $x_1 = x_2 = 0.5$, as well as the symmetry results from creating the equiprobability condition, we have

$$0.5 = y_1 + y_2 = y_2 + y_3 = \sum_{i=1}^3 \gamma_i z_i$$

We also have that the degeneracy factors are $\beta_2 = \gamma_2 = \gamma_5 = 2$, with all other β_i and γ_i set to 1. At equilibrium, with $\varepsilon_1 = 0$, we expect equiprobable distribution of the z_i among all possible states, so that we expect $z_1 = z_3 = 0.125$, as observed in Figure 12. Additionally (not shown in the figure), we would expect that $2z_2 = 0.250$, so that $z_1 + 2z_2 + z_3 = 0.5$.

6.2 Configuration variables: $\varepsilon_1 < 0$ ($h < 1$)

At the left-hand-side of the preceding Figure 12, we have the case where $h = e^{2\varepsilon_1} < 1$. These small values for h means that ε_1 , the interaction enthalpy between two unlike units (**A-B**), is negative. This further means that we stabilize the system by providing a structure that emphasizes alternate units; that is, by creating grid structures that look like **A-B-A-B**.

Note that in this realm, the pairwise combination y_2 (**A-B**) increases beyond the nominal expectation (when there is no interaction energy), so that $y_2 \rightarrow 0.5$, notably when $h < 0.4$.

As a natural consequence of the increase in y_2 when $h \rightarrow 0$, we also have $z_3 \rightarrow 0.5$ (maximizing **A-B-A** triplets) and also $z_1 \rightarrow 0$ (minimizing **A-A-A** triplets). (Note that a divergence in the analytic solution means that we do not have analytic values for the various configuration variables for small values of h .)

6.3 Configuration variables: $\varepsilon_1 > 0$ ($h > 1$)

Consider the case of a positive interaction energy between unlike units (the **A-B** pairwise combination). This is the case on the right-hand side of Figure 12, where $\varepsilon_1 > 0$ then yields $h = e^{2\varepsilon_1} > 1$.

The positive interaction energy ($\varepsilon_1 > 0$) suggests that a preponderance of **A-B** pairs (y_2) would destabilize the system, as each **A-B** pair would introduce additional enthalpy to the overall free energy. We want to bring the system to equilibrium, which is the free energy minimum. We would thus expect that as ε_1 increases as a positive value, we would see a decrease in y_2 , and also see smaller values for those triplets that involve non-similar pair combinations. That is, we would expect that the **A-B-A** triplet, or z_3 , would approach zero.

This is exactly what we observe this on the right-hand side of the Figure 12.

Thus, when $h \gg 1$ (or $\varepsilon_1 \gg 0$), we see that z_3 falls towards zero, and y_2 decreases as well. Note that y_2 can never go towards zero, because there will always be some **A-B** pairs in a system that contains units in a mixture of states **A** and **B**.

Correspondingly, this is also the situation in which $z_1 = z_6$ becomes large; for example, we see that $z_1 > 0.4$ when $h > 3.0$. (In fact, the analytic solution suggests that $z_1 = z_6 = 0.5$, which we know is not feasible; as mentioned earlier, the analytic solution is not accurate for extrema values of h .)

Notice that z_1 cannot truly approach 0.5, as z_3 did for the case where $h \ll 1$. The reason is that z_1 represents **A-A-A** triplets, and we will always have some **A-A-B** and **B-A-A** triplets, because we have an equiprobable distribution of units into states **A** and **B**. Thus, while we could conceivably have constructed a system composed exclusively of **A-B-A** and **B-A-B** triplets, we cannot do so exclusively with **A-A-A** and **B-B-B** triplets.

Despite this limitation, the realm of $h \gg 1$ is one in which we observe a highly structured system where large “domains” of like units mass together. We would expect these large domains (each comprised

of either overlapping **A-A-A** or **B-B-B** triplets) to stagger against each other, with relatively few “islands” of unlike units (e.g., the **A-B-A** and **B-A-B** triplets).

In actuality, the patterns that emerge for relatively high *h-values* still contain “spiderlegs” composed of triplets of unlike units. The actual observed topographies are discussed later in this work.

7 Interpreting the computational results

One important question, since we are taking a simple computational “find-and-flip” for finding the free energy minimum in a 2-D CVM grid, is the relative stability and depth of the free energy solution. One way to approach this is with a *perturbation study*, so that we take the following steps:

1. *First free energy minimization*,
2. *System perturbation*, and
3. *Second free energy minimization*.

The following subsections discuss the results of this study. We pay particular attention to how the various configuration variable values change as a response to *h*.

Some of the following was originally presented in the V & V document [25]. They are given again here (with both some contraction as well as expansion on certain points), to assist understanding of how the various configuration variable and thermodynamic values depend on the *h-value*.

7.1 Configuration variables and thermodynamic values: exemplar code run

Figure 13 presents an example result from the *perturbation studies* experiments. These results were initially presented in the V&V Report [25].

This data is actually from a perturbation run, where the 2-D grid is established as described via random pattern generation (see the V&V document for details), and then perturbed by a given amount (in this

case, a fraction of 0.1 of the existing nodes are flipped), and then taken to free energy minimum a second time.

What is interesting about this example, in comparison to previous analytic and computational results (see, e.g., Figure 11), is that it presents data for the case where $x_1 = 0.35$, and correspondingly, $x_2 = 0.65$. (By contrast, almost all previous discussions have dealt with the equiprobable case, where $x_1 = x_2 = 0.5$.)

When nodes are “flipped”, and as the resultant system is taken back to a free energy minimum, the process ensures that the total number of nodes in each of the two states, **A** and **B**. In this particular example, this means that the value of $x_1 = 0.35$ is maintained throughout.

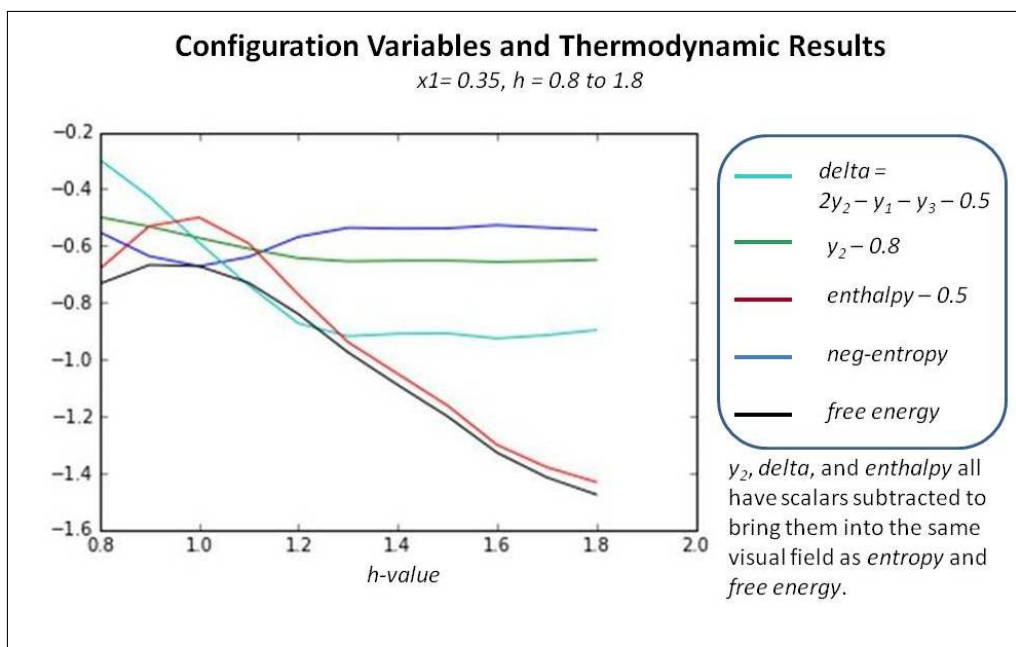


Figure 13: Configuration variable and thermodynamic values for the case where $x_1 = 0.35$ and $x_2 = 0.65$, and where the interaction enthalpy parameter h ranges as $h = 0.8..1.8$.

These results were obtained from the program 2D-CVM-perturb-expt-1-2b-2018-01-12.py, run on Friday, Jan. 12, 2018.

The parameter settings were for $x_1 = 0.35$ and $h = 0.8..1.8$, with a total of twenty trials ($numTrials = 20$) for each h -value. The data table from this run is presented in the V&V Report [25]. All

reported results for configuration variable and thermodynamic values are averages over $numTrials$ runs, where $numTrials = 20$.

7.2 Interpreting the y_2 results

The values observed for y_2 conform to expectations. In Figure 13, y_2 is shown in green, as $y_2 - 0.8$ (in order to bring the y_2 values within the same visual range as other results). (More details are given in the previously-mentioned V&V document [25].)

When $h = 1.0$, $y_2 = 0.2278$, which is the expected result. (The true expected result is $y_2 = 0.35 * 0.65 = 0.2275$; the observed value of 0.2278 is an average over twenty trials. The deviance from the theoretical expectation is acceptable.)

When $h < 1.0$, the y_2 values are greater, and when $h > 1.0$, the y_2 values are smaller. In fact, y_2 ranges from $y_2 = 0.301$ (when $h = 0.8$) down to $y_2 = 0.151$ (when $h = 1.8$). These again are expected results. In brief, when $h < 1.0$, then $\varepsilon_1 < 0.0$, meaning that the interaction enthalpy parameter ε_1 is negative. When ε_1 is negative, the enthalpy is decreased by increasing y_2 , as the interaction enthalpy ε_1 multiplies the term $(2y_2 - y_1 - y_3)$. Thus, maximizing y_2 is expected when $h < 1.0$.

There is a limit as to how far y_2 can be increased; presumably it can approach 0.5, however, that would mean that the units were arranged in a strict checkerboard manner; that there were no instances of like-near-like at all. This is rather difficult to achieve; both in creation of highly-ordered systems, and in this particular code, which uses a simplistic *find-and-flip* strategy.

As previously noted, when $h > 1.0$ ($\varepsilon_1 > 0.0$), the y_2 values are smaller. This is because the system enthalpy now is decreased when y_2 is made smaller. Thus, the system moves more towards a like-with-like configuration (increasing y_1 and y_3); maximizing the size of the various “islands,” and decreasing the size of their borders (minimizing y_2).

There is a practical limit as to how far y_2 can be decreased; there will always be a border area between the state **A** islands (or even a single, massive state **A** continent) and the surrounding sea of state **B** units. This means that y_2 will not get close to zero. The actual practical limit for y_2 will actually depend on the total system size (total number of nodes), because the border area will progressively decrease (although not disappear) as more and more islands join to become continents. Thus, the value of $y_2 < 0.157$, which occurs when $h \geq 1.2$, is not surprising.

Once y_2 is pushed to a suitably small value, it becomes increasingly difficult for the simple *find-and-flip* strategy to (randomly) find nodes where the flip will accomplish a free energy reduction. This is likely why there is general stability in the y_2 values beyond $h \geq 1.2$; there are simply not that many nodes where the flip will do much good, keeping in mind that *two* nodes (each in a different state) have to be flipped in order to maintain the x_1 value.

Thus, the preliminary conclusion is that free energy minimization is being accomplished, and that the y_2 values are behaving as expected.

7.3 Interpreting the *delta* results

Again referencing Figure 13, we examine the curve for *delta* (shown in cyan), defined as $(2y_2 - y_1 - y_3)$, which is the actual term that is multiplied by ε_1 to achieve the interaction enthalpy term. (The contributing term for y_2 is shown in dark green in this figure.) This curve behaves as expected.

In particular, we note that there is a nearly linear behavior in the region between $h = 0.8$ and $h = 1.3$. When $h = 0.8$, $delta = 0.2035$ (according to the data table shown in V&V document [25]). When $h = 1.2$, $delta = -0.3730$. When $h = 1.0$, we would expect that there would be purely probabilistic distribution of units into their configurations, and thus expect that $y_1 = 0.35 * 0.35 = 0.1225$, $y_3 = 0.65 * 0.65 = 0.4225$, and $y_2 = .2275$ (as mentioned earlier). We would have then that $2y_2 - y_1 - y_3 = 2 * .2275 - 0.1225 - 0.4225 = -0.090$. The actual value is $delta = -0.0887$, which is acceptably close.

Similar arguments hold for the expected and observed values of *delta* as did for y_2 in the preceding discussion.

We again note that the values for *delta* level out as h increases beyond 1.2; this is because there are not that many units that the simple *find-and-flip* strategy can easily find. In particular, we note that the z_3 value at $h \geq 1.3$ is typically around $z_3 = 0.04$, which is very small.

In particular, we observe that this z_3 value indicates that we have pushed the system to its limit for minimizing z_3 , which is the **A-A-B** configuration. This z_3 value indicates a border of a rather large island of state **A** units in a sea of **B** units. Specifically, for the 256-unit system that is the subject for this investigation, when $z_3 = 0.04$, then $N = 0.4 * 256 / 2 = 102.4 / 2 = 51$ triplets involve border units around islands / continents of state **A**. This is approximately *1/5th* of the

total number of units available. This suggests that we have pushed the system about as far as it can go. Of course, a visual inspection of the resulting grid would be enormously useful in confirming these assessments. This will be included in a subsequent document.

7.4 Interpreting the thermodynamic results

The enthalpy curve is shown in red in Figure 13. (Actually, the curve shown is *enthalpy-0.5*, so that it can be seen in close juxtaposition to the other data presented.)

The enthalpy is maximum when $h = 0$, which is to be expected. As we minimize free energy, we minimize enthalpy. As soon as we introduce some non-zero interaction enthalpy, we have an opportunity to adjust the configuration values (specifically the y_i , as just discussed) to lower the enthalpy.

The entropy is similarly at a maximum (neg-entropy is at a minimum) when $h = 0$. The negative entropy increases for non-zero values of h , as expected.

We particularly note that in the vicinity of $h = 0$, or more generally, in the range of $0.8 \leq h \leq 1.3$, the variances in the entropy and enthalpy are approximately on the same scale; one does not appreciably dwarf the other.

When we move beyond $h \geq 1.3$, we find that the enthalpy term strongly dominates the entropy, and thus dominates the free energy. It does this because we are increasing the value of the interaction enthalpy coefficient, ε_1 , and not because we are gaining any appreciable difference in the configuration values. As noted in the previous discussions, these values have more-or-less stabilized in this range.

Thus, **increasing h beyond $h = 1.3$ does not serve any useful value**, suggesting a practical bound on h -values for this kind of system.

Our actual and practical choices for the h -values should be based on the kind of behavior that we want to see in the configuration values. For modeling brain-like systems, we will most likely want $h \geq 0$, as that induces *like-with-like* clustering, which seems to characterize certain neural collectives.

In summary, the most useful result of the *perturbation studies* has been to not only confirm that the various configuration variables and thermodynamic values behave as expected (which is why these results were included in the earlier V&V study [25]), but also a **practical bound on the upper range for the h -value**, i.e., $h < 1.3$.

8 The phase space: boundary values

The previous sections introduced the configuration variables and the free energy for the 2-D CVM. What we would now like to obtain is a mapping of a set of configuration variable values to a corresponding *h-value*.

The phase space that we wish to describe has two boundaries:

- Activation enthalpy is zero ($\varepsilon_0 = 0$), and
- Interaction enthalpy is zero ($\varepsilon_1 = 0$).

We have already given substantial attention to the first case, where $\varepsilon_0 = 0$. This is the case where we have equiprobable units in each state, **A** and **B** ($x_1 = x_2 = 0.5$). We found the analytic solution giving the values for each of the configuration variables in this case, and also identified that the analytic solution has a divergence. Thus, we have identified a *protocol* for obtaining the actual configuration variables for a given *h-value*, when $\varepsilon_0 = 0$.

What this gives us is a means of computationally obtaining the approximate configuration variables corresponding to a given *h-value*; limited by the constraint that $\varepsilon_0 = 0$. We also have an approximate upper bound on a useful value for *h-value*; this is not a hard limit, but it suggests that going much further for the *h-values* will not give us substantially further value.

We have not yet discussed the second case, in which the interaction enthalpy is zero, except for a brief example in Subsections 7.2 and 7.3. As a brief overview, when the interaction enthalpy $\varepsilon_1 = 0$, then the distribution of the configuration variables can be found on a strictly probabilistic basis.

This in itself is straightforward and expected.

What is not obvious, from this correlation, is the relationship between x_1 and the activation enthalpy parameter ε_0 .

That is, we know that as ε_0 increases, the corresponding free energy-minimized value for x_1 should decrease. This is because the overall free energy is minimized when we reduce the number of active units (state **A** units) as we associate more and more energy (enthalpy) with those active units.

Fortunately, we can obtain this correlation.

This is addressed in a subsection immediately following the next, which reviews the impact of the interaction enthalpy parameter. First, we address the task of finding a reasonable *target h-value*.

8.1 Phase space boundary: activation enthalpy is zero

When the activation enthalpy $\varepsilon_0 = 0$, then we have the situation described in the previous sections.

Given a value for ε_1 , we can analytically obtain the various configuration variable values. However, as we've previously discussed, these analytically-obtained values are in error, especially as we increase $\varepsilon_1 > 0$ (or $h > 1$).

More often, we are likely to start with a 2-D CVM grid that is not at equilibrium, and the various configuration variables do not align neatly with a single corresponding *h-value*.

This means that we need a *Protocol* for taking a system to a free energy equilibrium point. (Such a *Protocol* was briefly identified in the preceding section.) Once we've taken a system to a free energy minimum, we can then identify the configuration variables associated with that free energy-minimized grid.

However, before we can do this needed free energy minimization, we need some starting point - we need an estimated or *target h-value*, which will guide the free energy minimization process that starts with the initial 2-D CVM grid configuration.

Once the free energy minimization is complete, the *target h-value* has become the *actual h-value*, and the configuration variable values have adjusted so that the free energy minimization is satisfied for that particular *h-value*. That is, the configuration variable values that are obtained as a result of free energy minimization will be approximately those that are associated (in a real sense) with the corresponding *h-value*. These configuration variable values may differ from those of the analytic solution.

Thus, given an initial grid configuration, our first step is to find a good *target h-value*.

We can identify our *target h-value* by any of a variety of means. One very simple approach is to identify the approximate *h-value* corresponding to different measured (counted) configuration variable values, e.g., z_1 , z_3 , and y_2 . (Figure 7 illustrated select counted (Z_1 and Z_3) and fractional (z_1 and z_3) computational variable values for an initial grid.) We can then take either an average of these different corresponding *h-values* or even select a visual approximation. The way in which we do this is not very important at this stage, as we're going to change the configuration variables substantially as we bring this initial starting

grid to a free energy minimum.

Later, when we have a good set of correspondences between (at-equilibrium) configuration variable values and their corresponding *h-values*, we can use a table look-up to find a good *target h-value*. However, we've not yet established this full set of correspondences.

If we want a more mathematical approach, we can obtain an approximate *h-value* by using an analytic method, described in Appendix B.

Regardless of the method that we use, the *h-value* that we've selected becomes a **target** *h-value*; that is, we will drive the system to a grid configuration that is at an equilibrium point for *that specific h-value*.

Once we've identified an initial 2-D CVM grid configuration and a *target h-value*, we carry out a computational process of free energy minimization, which requires selecting and flipping various nodes (from **A** to **B**, and vice versa). Throughout this process, we keep the relative ratio of nodes in states **A** and **B** constant.

For the equiprobable case where we have $x_1 = x_2 = 0.5$, we could have hoped that the analytic values for the configuration variables would be approximately correct, especially when ε_1 is close to 0 (h is close to 1.0). However, as detailed results in Appendix D show, the at-equilibrium configuration variable values are substantially different from those predicted by the analytic solution, even for *h-values* reasonably close to $h = 1$.

Thus, our first goal is to build out a set of configuration variable values associated with corresponding *h-values*, which is shown as the vertical (LHS) axis in Figure 14.

The best way to figure out the configuration variable value sets associated with different *h-values* (that is, figure out values along the LHS axis of Figure 14) is to start with some initial grid configuration, pick a *target h-value*, and then conduct free energy minimization. Then, the resulting values for the different configuration values (as averaged over multiple runs) should be useful.

Naturally, the trick is to pick a good *target h-value* for a given initial grid.

Appendix B walks through this process in some detail, and further discusses the topographies associated with different *h-values*.

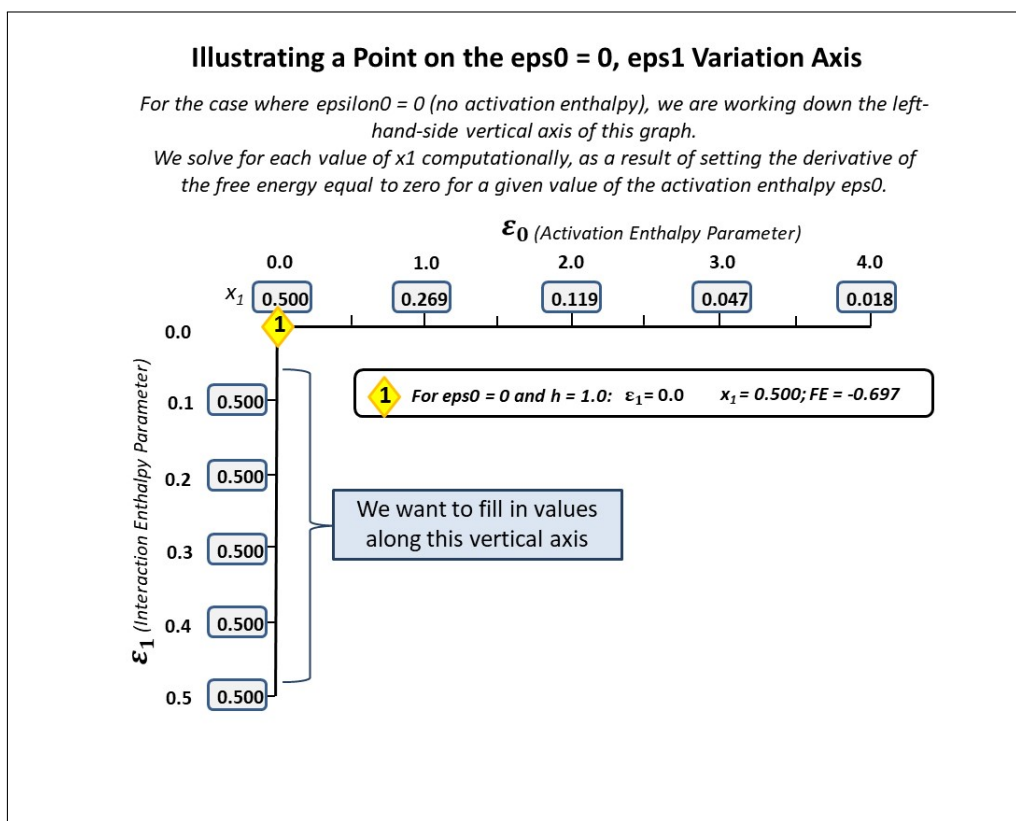


Figure 14: The first step is to identify the configuration variable and thermodynamic values along one axis; in this case, where we keep $\epsilon_0 = 0$ and vary ϵ_1 (or vary h).

8.2 Phase space boundary: interaction enthalpy is zero

When the interaction enthalpy $\epsilon_1 = 0$, then we have the phase space boundary depicted by the upper axis of Figure 14.

Along this axis, the values of the configuration variables y_i , w_i , and z_i are probabilistically determined by the value of x_1 . This is because the values for the configuration variable values other than that for x_1 vary from their respective randomly-defined values *only* because the interaction enthalpy brings like terms together, or pushes them apart (depending on the interaction enthalpy parameter value for ϵ_1 , or correspondingly, when $h \neq 1.0$).

When $h = 1.0$, then there is no reason for the distribution of unit states to differ from random. (Unless, of course, the activation enthalpy $\varepsilon_0 > 0$, in which case we'll have a smaller number of units in state **A** ($x_1 < 0.5$). Even then, the values for all the other configuration variables will be defined by the value for x_1 .)

We can define a reasonable extent for the upper (horizontal) phase space boundary axis, where $x_1 \approx 0.05$, because when x_1 has that value, we have the following values for certain other configuration variables:

- $x_1 = 0.5$ - total number of units in state **A** = $0.5 * N$, where N is the total number of units in the grid. When $N = 256$ (a 16x16 unit grid), $X_1 = 0.5 * 256 = 128$, which is readily achieved.

Appendix C presents details for computing the configuration values along the upper horizontal ($\varepsilon_1 = 0$ axis), including the mechanism for identifying the x_1 value that correlates with specific values of ε_0 .

8.3 Phase space: useful extent

Based on the results from the previous two sections, we can now identify the *useful extent of the phase space boundaries* for the 2-D CVM. These are summarized in Figure 15.

8.4 Phase space interior: need for incremental approach

In the previous two sections, we identified an overall approach for obtaining both configuration variable and thermodynamic values across the two phase space boundary edges; i.e., where either $\varepsilon_0 = 0$ or $\varepsilon_1 = 0$.

Now, we're interested in the interior of the phase space; in points such as that shown in Figure 16.

The next step is to identify the configuration variable and thermodynamic values for the phase space interior; i.e., when both the interaction enthalpy and the activation enthalpy are greater than zero. This figure shows one known point along the upper horizontal axis, where $\varepsilon_1 = 0.0$, and $\varepsilon_0 = 1.0$. For this pair of enthalpy parameters, $x_1 = 0.269$.

In general, along this upper horizontal axis, the non-zero values for ε_0 mean that we have $x_1 < 0.5$. For the specific point illustrated

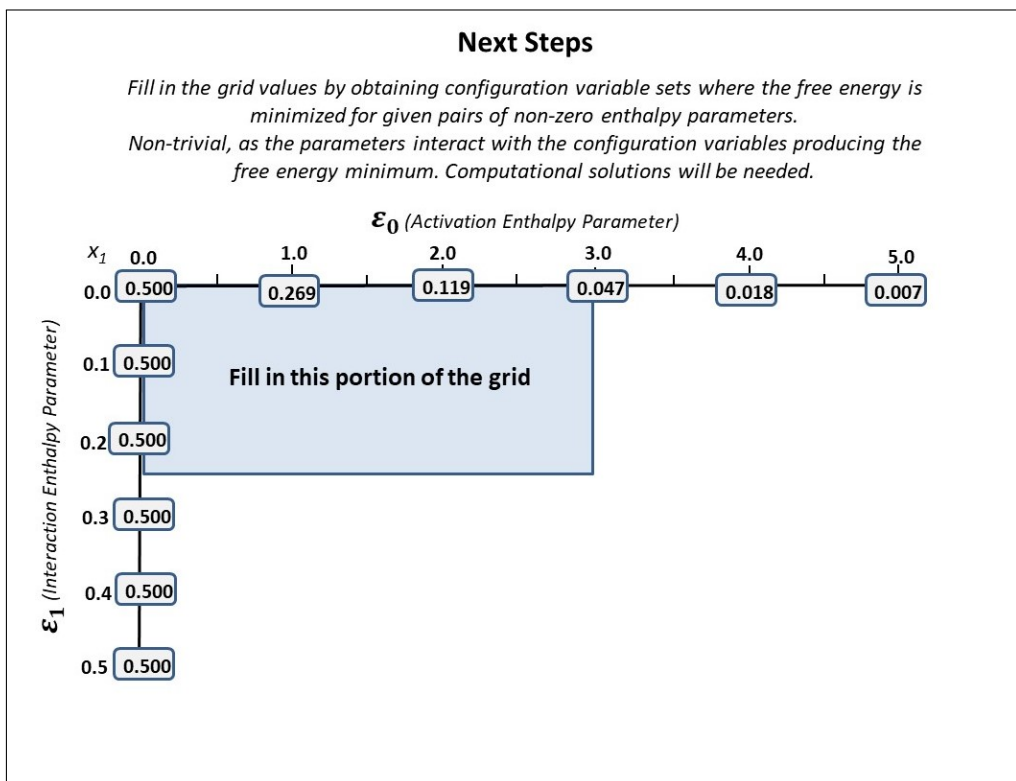


Figure 15: The useful extent for the phase space boundaries. The useful range for ϵ_1 (when $\epsilon_0 = 0$, down the LHS axis) is $\epsilon_1 = 0.0 \dots 0.5$ (or $h = 1.0 \dots 1.5$). Along the upper horizontal axis, we hold $\epsilon_1 = 0$ and vary ϵ_0 along the range $\epsilon_0 = 0.0 \dots 3.0$.

in Figure 16, we obtained the exact value for x_1 following a protocol identified in the previous section.

It is not as straightforward to identify the configuration variable values when we have non-zero values for both ϵ_0 and ϵ_1 . This is the kind of situation illustrated in Figure 17.

This kind of system is illustrated in Figure 18, which shows an initial grid structured as a very small rich club.

Previous experiments with “rich-club-like” topographies showed us that even with high values for ϵ_1 , we still found that the initial grid design was disrupted as we brought the system to equilibrium. Thus,

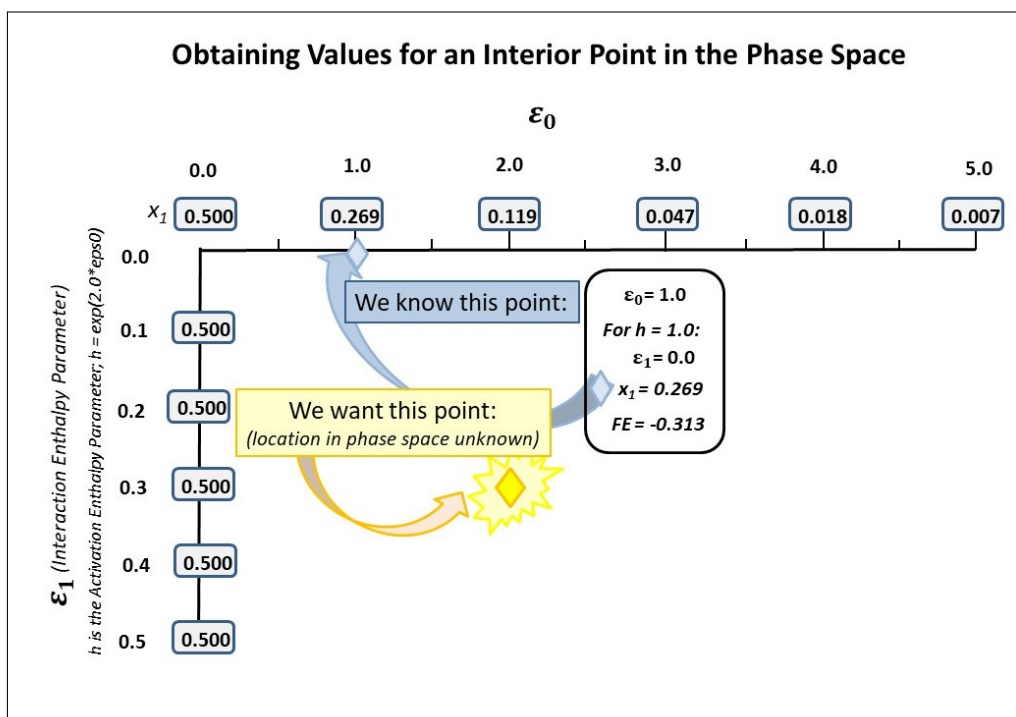


Figure 16: The next step is to identify the configuration variable and thermodynamic values for the phase space interior; i.e., when both the interaction enthalpy and the activation enthalpy are greater than zero. This figure shows one known point along the upper horizontal axis, where $\varepsilon_1 = 0.0$, and $\varepsilon_0 = 1.0$.

we anticipate that the system shown in Figure 18 is not at equilibrium.

The challenge in bringing such a system to equilibrium is that we need to specify, in advance, the values for both ε_0 and ε_1 .

In this case, we don't know either of these enthalpy parameters. We know that both of them will be greater than zero. We suspect that the value for ε_0 will be in the neighborhood of 2.0, because for this manually-designed system, $x_1 = 30/256 = 0.117$, and we know that if $\varepsilon_1 = 0.0$, then $x_1 = 0.119$ when $\varepsilon_0 = 2.0$. However, we don't know as yet how the configuration values change as we increase *both* ε_0 *and* ε_1 .

To accomplish our goal, we would need to establish an initial grid, such as is shown in Figure 18, and iteratively solve (varying not only the two enthalpy parameters but also the x_1 values) for a free energy minimized system. This will be the subject of a future study.

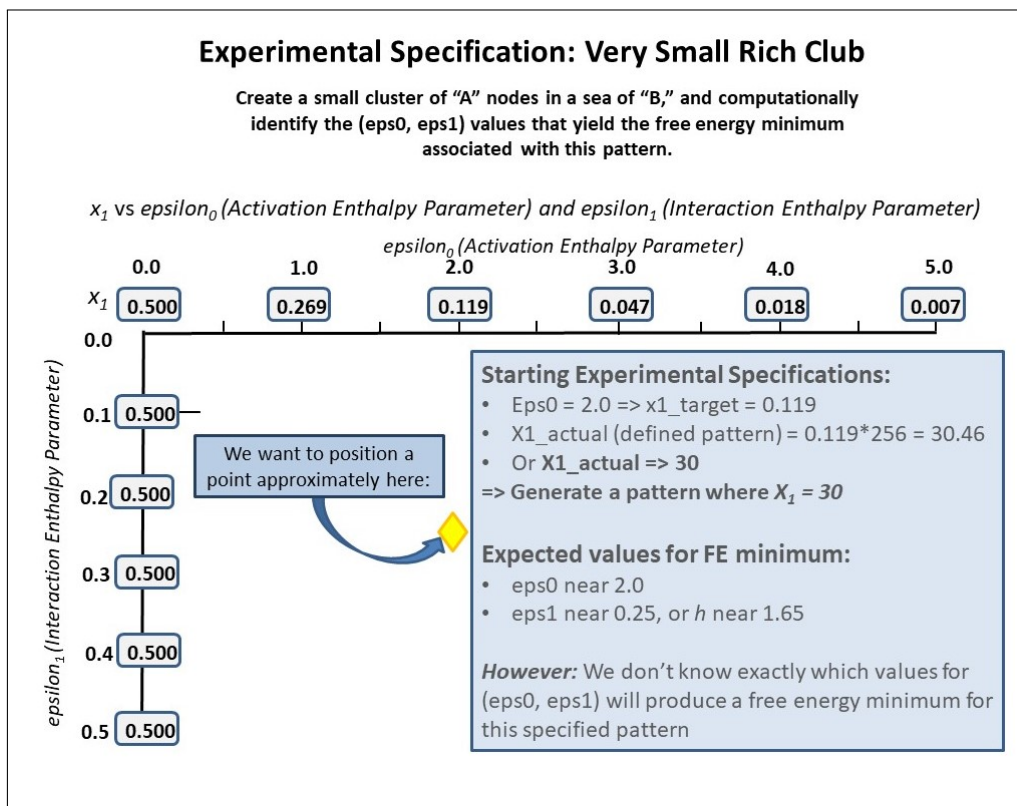


Figure 17: We want to find the configuration variable values for points where the enthalpy parameters are in the phase space interior, so that both $\epsilon_0 > 0.0$ and $\epsilon_1 > 0.0$.

9 Summary and conclusions

There are several things that we can conclude from this preliminary investigation:

- **Analytic vs. computational results** - while there is an analytic solution (when $x_1 = x_2 = 0.5$), this analytic solution has two divergence points. We would expect that the computational values for the configuration variables would differ as the h -value approaches the divergence points. What is surprising is that the computational results differ from the analytically-predicted ones much earlier than would be expected.
- **Useful range of the ϵ_0 enthalpy parameter** - this study did

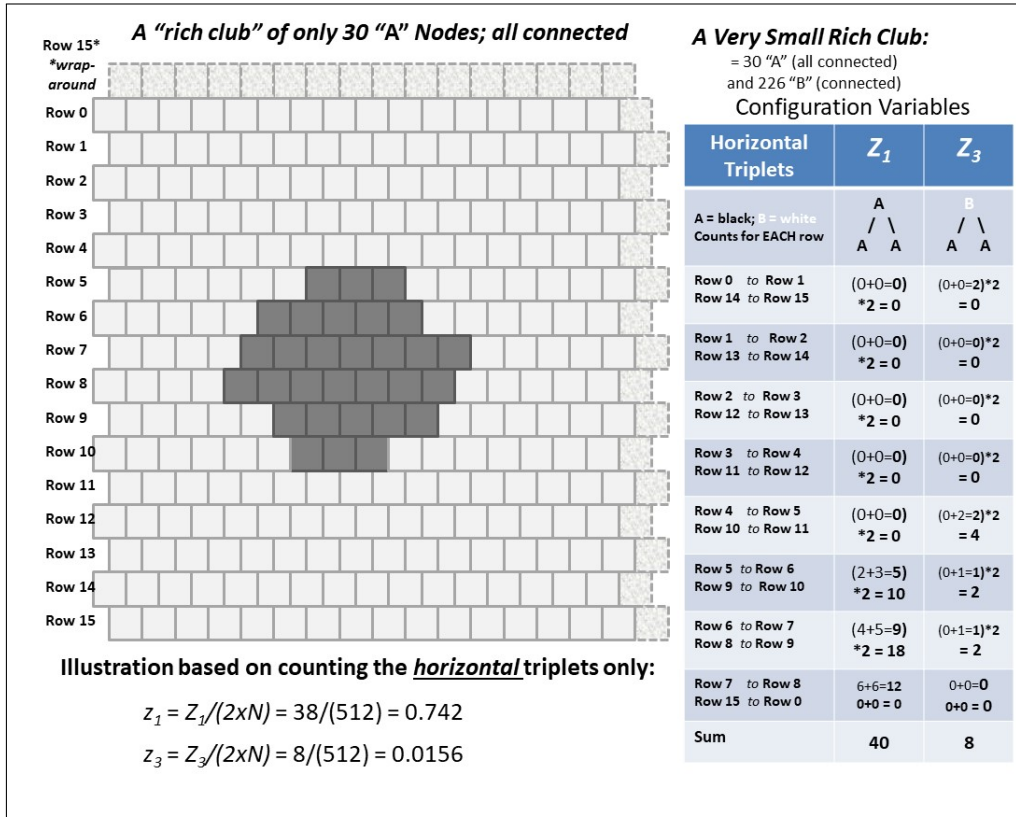


Figure 18: An initial grid consisting of a very small rich club, or single small mass of 30 **A** units. We would anticipate that the enthalpy parameters would be somewhere in the neighborhood of $\varepsilon_0 = 2.0$, and $\varepsilon_1 > 1.5$.

not go so far as to computationally confirm the configuration variables given certain values of ε_0 . Rather, we have identified how (when $\varepsilon_1 = 0$) x_1 and other configuration variables correlate with ε_0 . We still need to take these values and confirm them computationally. However, this correlation between ε_0 and x_1 gives us a useful range for ε_0 . While this range depends (somewhat) on the grid size, it is reasonable to keep $\varepsilon_0 < 3$, and possibly smaller.

- **Useful range of the ε_1 enthalpy parameter** - we can similarly identify that a useful range for $\varepsilon_1 < 2$, and again, possibly smaller. A study reported in Subsection 7.2 suggests that even values up

to $h = 1.3$ may be more than necessary, although larger h -values (e.g., $h = 1.65$) were used in the course of this work and did indeed produce notably different results compared with smaller h -values (e.g., $h = 1.16$).

In addition to these basic findings, we note interesting properties in the 2-D topographic grids that are generated during the free energy minimization process - topographic features such as “spider-legs,” “channels,” and “rivers.” The whole notion of free-energy-based topographies is new and worth substantial future study.

10 Future directions

There are numerous steps to be taken:

- **Map the phase space** - we need the full set of configuration variable values associated with parameter sets $(\varepsilon_0, \varepsilon_1)$.
- **Smart strategies** - once we know the target configuration variables associated with a given parameter set, we can evolve smart strategies to move in the direction of a known solution.
- **Topography characterization** - as we understand the topographies induced by different parameter sets, we can begin correlating free energy-based topographies with various kinds of observable 2-D patterns, ranging from physical landscapes to brain activation patterns.

The most immediate step, which will enable the tasks just identified, will be **object-oriented code development** - a necessary and obvious next-step. This will allow us to associate various properties with each unit (node) in the grid, and that will make possible the evolution of smart strategies for free energy minimization processes, instead of the simple find-and-replace method currently used.

All of these are necessary preliminaries. Once completed, we can investigate use of a 2-D CVM grid and the associated free energy minimization process within a new form of computational engine.

11 Code referenced in this document

- **2D-CVM-perturb-expt-1-2b-2018-01-12.py** - free energy minimization including perturbation after reaching the first free

energy minimum; this allows confirming that the free energy minimum is stable; allows user-specifiable (in `**main**`) values for x_1 , h , $numTrials$, and many other parameters.

- **2D-CVM-def-pttrns-anlytc-FE-vary-e0-and-e1-2018-12-12.py**, **2D-CVM-def-pttrns-anlytc-FE-vary-e0-and-e1-v1pt1-2018-12-29.py**, and **2D-CVM-def-pttrns-anlytc-FE-vary-e0-and-e1-v1pt3-2018-12-29.py** (Note: the actual program files have underscores in place of some of the hyphens used in the filename just given; the filenames MAY be updated when the code is released) - free energy minimization given a starting user-defined 2-D grid, together with user-specified values for x_1 and ε_1 (the *h-value*). Different programs perform slightly different tasks, with the same overall structure.

Code Availability: Codes referenced here may be made available in the future. The code will be supported by extensive documentation, which will also be placed in the GitHub repository. Inquiries should be directed to: alianna@aliannajmaren.com. The verification and validation for the codes used to produce results presented here is given in Maren (2019) [25]. The best way to be informed of future developments is to “opt-in” on the author’s website, at www.aliannajmaren.com.

Copyright: All codes referenced here have been independently developed by A.J. Maren. A.J. Maren holds the copyright to both the codes and this document itself. arXiv is granted a non-exclusive and irrevocable license to distribute this article.

A Appendix A: The 2-D CVM Equation

This appendix recapitulates the free energy formalism for the 2-D CVM grid originally made by Kikuchi in 1951 [1], and further refined by Kikuchi and Brush in 1967 [2] (Eqn. I.16). Following their approach, we treat the 2-D CVM grid as being constructed from a series of zigzag chains.

We begin with the free energy equation, previously introduced in Section 5.2 as Eqn. 4, and repeated here for convenience as

$$\begin{aligned}
\bar{G}_{2-D} = G_{2-D}/N = & \\
& \varepsilon(-z_1 + z_3 + z_4 - z_6) - \bar{S}_{2-D} \\
& + \mu(1 - \sum_{i=1}^6 \gamma_i z_i) + 4\lambda(z_3 + z_5 - z_2 - z_4)
\end{aligned} \tag{A-1}$$

where the entropy, previously expressed as Eqn. 15, is also repeated here as

$$\bar{S}_{2-D} = 2 \sum_{i=1}^3 \beta_i Lf(y_i) + \sum_{i=1}^3 \beta_i Lf(w_i) - \sum_{i=1}^2 Lf(x_i) - 2 \sum_{i=1}^6 \gamma_i Lf(z_i), \tag{A-2}$$

and where $Lf(v) = v \ln(v) - v$. The Lagrange multipliers are μ and λ , and we have set $k_\beta T = 1$.

As noted previously in Section 5.1, we are working with two terms in the enthalpy expression; the activation enthalpy and the interaction enthalpy.

We base the interaction enthalpy term in this equation on the expression introduced first by Kikuchi and Brush [2] (Eqn. I.16), who express the enthalpy for the 2-D CVM as

$$\bar{H}_{2-D} = 2\varepsilon_1(2y_2 - y_1 - y_3) = 2\varepsilon_1(-z_1 + z_3 + z_4 - z_6), \tag{A-3}$$

using the equivalence relations

$$y_1 = z_1 + z_2 \tag{A-4a}$$

$$y_2 = z_2 + z_4 = z_3 + z_5 \tag{A-4b}$$

$$y_3 = z_5 + z_6. \tag{A-4c}$$

This expresses the notion that the interaction enthalpy is identified as twice the value of each nearest-neighbor interaction (y_i). (The multiplier in front of the y_2 term is due to the double degeneracy of y_2 .)

If the interaction enthalpy parameter ε_1 is positive, then we reduce the overall free energy by increasing the relative proportion of nearest-neighbor interactions between those that are like each other (y_1 and y_3 , or **A** - **A** and **B** - **B**, respectively), and decreasing the

relative proportion of interactions between unlike nodes (y_2 , or **A - B** interactions). Conversely, if the interaction enthalpy ε_1 is negative, we minimize the free energy by increasing the proportion of unlike nearest neighbor pairs (increasing y_2). When $\varepsilon_1 = 0$, the configuration variables should all be at what would be expected from random distribution. Specifically, for the case where $x_1 = x_2 = 0.5$, we would expect that $2y_2 = 0.5$, and $y_1 = y_3 = 0.25$.

A.1 Equivalence Relations Among the Configuration Variables

For completeness, we present the entire set of equivalence relations among the configuration variables. This means that we express the sets of x_i , y_i , and w_i in terms of the z_i (Eqns. I.1 - I.4 [2]):

For the y_i :

$$y_1 = z_1 + z_2 \tag{A-5a}$$

$$y_2 = z_2 + z_4 = z_3 + z_5 \tag{A-5b}$$

$$y_3 = z_5 + z_6. \tag{A-5c}$$

For the w_i :

$$w_1 = z_1 + z_3 \tag{A-6a}$$

$$w_2 = z_2 + z_5 \tag{A-6b}$$

$$w_3 = z_4 + z_6 \tag{A-6c}$$

For the x_i :

$$x_1 = y_1 + y_2 = w_1 + w_2 = z_1 + z_2 + z_3 + z_5 \tag{A-7a}$$

$$x_2 = y_2 + y_3 = w_2 + w_3 = z_2 + z_4 + z_5 + z_6 \tag{A-7b}$$

The normalization is:

$$1 = x_1 + x_2 = \sum_{i=1}^6 \gamma_i z_i. \tag{A-8}$$

A.2 Microstates for the 1-D CVM

We begin with describing the 1-D CVM, constructed as a single zigzag chain, illustrated previously in Figure 2. We consider how we can construct a 1-D CVM system, composed as a single zigzag chain, originally presented as Figure 2 in Kikuchi and Brush [2], and shown here as Figure 19. Following the notation introduced by Kikuchi and Brush, we allow (in this section) N_2 to be the number of nodes per single row.

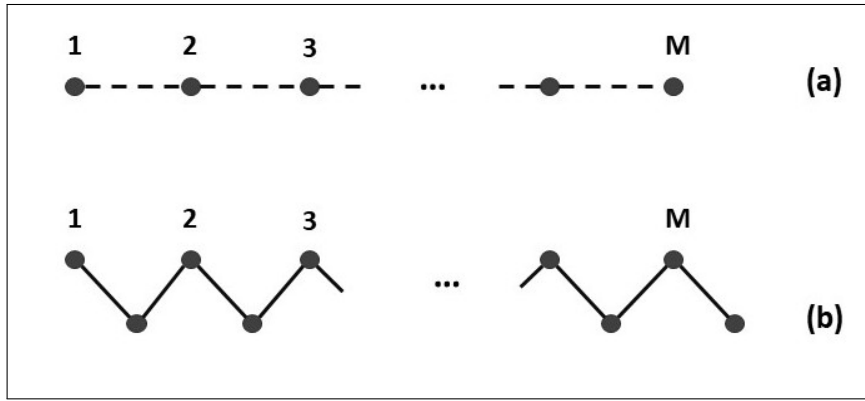


Figure 19: A horizontal single row (a) and a double row (b), from a square lattice CVM grid, turned to the diagonal; originally presented as Figure 2 in Kikuchi and Brush [2].

Viewing the zigzag chain as being composed of two horizontal rows, the number of ways of constructing a *single row* of this chain are given as (Eqn. I.7 - 1.8 [2])

$$\Omega_{single} = \frac{\{point\}_M}{\{diagonalpair\}_M}, \quad (\text{A-9})$$

where

$$\{point\}_M = \prod_{i=1}^3 (Mx_i)! \quad (\text{A-10})$$

and

$$\{diagonalpair\}_M = \prod_{i=1}^3 (Mw_i)^{\beta_i}. \quad (\text{A-11})$$

A.3 Microstates for the 2-D CVM

Referring now to Figure 19(b), we note that it is a zigzag form connecting two adjacent rows. This essentially constitutes a 1-D CVM system, and the number of ways of constructing this system can be derived similar to the previous equations, and is given as

$$\Omega_{double} = \frac{\{pair\}_{2M}}{\{angle\}_{2M}}, \quad (\text{A-12})$$

where

$$\{pair\}_{2M} = \prod_{i=1}^3 (2My_i)^{\beta_i} \quad (\text{A-13})$$

and

$$\{angle\}_{2M} = \prod_{i=1}^6 (2Mz_i)^{\gamma_i}. \quad (\text{A-14})$$

As noted by Kikuchi and Brush (Eqn. I.11), when M is large, we can use Stirling's approximation to write Eqn. (A-16) as

$$\Omega_{double} = \left[\frac{\{pair\}_M}{\{angle\}_M} \right]^2. \quad (\text{A-15})$$

where M is the number of lattice points in a row, and Ω_{double} refers to the juxtaposition of two rows. The degeneracy factors β_i and γ_i were described in Section 3.1, and illustrated in Figure 4. (*Note:* This equation is identical with the original presentation given by Eqns. I.9 - I.10 from Brush and Kikuchi (1967) [2].)

When M is large, Stirling's approximation can be used to express the previous equation as (Eqn. I.11 from Brush and Kikuchi)

$$\Omega_{double} = \left[\frac{\prod_{i=1}^3 (My_i)^{\beta_i}}{\prod_{i=1}^6 ((Mz_i)^{\gamma_i})} \right]^2, \quad (\text{A-16})$$

where Stirling's approximation is given as: $N! = N \ln(N) - N$.

We now wish to construct a 2-D system by adding a series of rows on top of the initial 1-D system, composed as the initial zigzag chain.

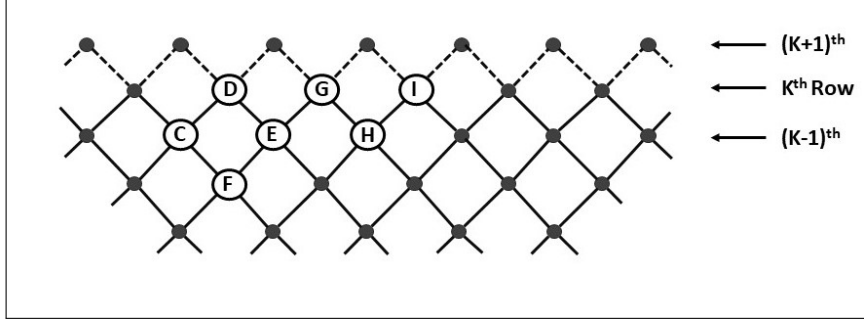


Figure 20: A 2-D CVM system, completed up to the K^{th} row, originally presented as Figure 1 in Kikuchi and Brush [2].

Suppose that the system has been completed up to the k^{th} row, as shown in Figure 20.

The number of ways in which we can add the $K + 1^{th}$ row, when the system has been completed to the K^{th} row, is the ratio $\Omega_{double}/\Omega_{single}$. Thus, the number of ways of adding a total of K rows and completing the entire system is (Eqn. I.12 from Brush and Kikuchi)

$$\Omega = \left[\frac{\Omega_{double}}{\Omega_{single}} \right]^K. \quad (A-17)$$

We can now substitute from Eqns. A-9 and A-16 into Eqn. (A-17), and use Stirling's approximation to obtain

$$\Omega = \frac{\{pair\}_{N^2} \{diagonalpair\}_N}{\{angle\}_{N^2} \{point\}_N}. \quad (A-18)$$

Kikuchi and Brush note that “The source of approximation in this expression lies in identifying Ω_{double} and Ω_{single} in Eqn. I.12 [Eqn. A-17] with those in (I.11) and (I.7) [Eqns. A-15 and A-9, respectively]. In order to be rigorous, the Ω 's in Eqn. I.12 [Eqn. A-17] should be constructed using an infinitely long zigzag form, as in Figure 2(b) [Figure 19(b)], for the basic cluster.”

We now wish to find an expression for the system entropy, which is defined as

$$S = k_\beta \ln \Omega. \quad (\text{A-19})$$

We substitute from Eqn. A-18, Eqn. A-11, and Eqn. A-14 into Eqn. A-19, and once again use Stirling's approximation to obtain the entropy for the system as

$$S_{2-D} = k_\beta \ln \Omega = k_\beta N \left[2 \sum_{i=1}^3 \beta_i Lf(y_i) + \sum_{i=1}^3 \beta_i Lf(w_i) - \sum_{i=1}^2 Lf(x_i) - 2 \sum_{i=1}^6 \gamma_i Lf(z_i) \right]. \quad (\text{A-20})$$

where $Lf(x) = x \ln(x) - x$, and k_β is Boltzmann's constant.

When we divide through by $k_\beta N$, we recover the reduced system entropy as given in Eqn. A-2. This is the entropy associated with a a full 2-D CVM grid.

A.4 Analytic Solution for the 2-D CVM: Establishing the Equilibrium Equations

Achieving the analytic solution involves solving a free energy equation for the equilibrium point, where the enthalpy-per-active-unit is given as zero, and the pairwise-interaction enthalpy is given as $\varepsilon = \varepsilon_1$. Because the enthalpy-per-active-unit is zero ($\varepsilon_0 = 0$), there is no a priori preference for a unit to be in either the **A** or **B** states; thus, $x_1 = x_2 = 0.5$.

Because states **A** and **B** are equiprobable, we have a symmetric distribution with the other configuration variables; specifically:

$$\begin{aligned} y_1 &= y_3 \\ z_1 &= z_6 \\ z_2 &= z_5 \\ z_3 &= z_4 \end{aligned} \quad (\text{A-21})$$

As a first step, we take the derivative of the free energy equation Eqn. A-1 with respect to each of the configuration variables z_i . This gives us

$$\begin{aligned}
z_1q &= e^{\beta\varepsilon}y_1(w_1/x_1)^{1/2} \\
z_2q &= e^{\lambda}(y_1y_2w_2)^{1/2}(x_1x_2)^{-1/4} \\
z_3q &= e^{-2\lambda}e^{-\beta\varepsilon}y_2(w_1/x_1)^{1/2} \\
z_4q &= e^{2\lambda}e^{-\beta\varepsilon}y_2(w_3/x_2)^{1/2} \\
z_5q &= e^{-\lambda}(y_2y_3w_2)^{1/2}(x_1x_2)^{-1/4} \\
z_6q &= e^{\beta\varepsilon}y_3(w_3/x_2)^{1/2}
\end{aligned} \tag{A-22}$$

where $q = e^{-\mu\beta/2}$, according to Kikuchi and Brush (Eqn. I.19), and (since we are working with reduced equations) we set $\beta = 1$, so that we have $q = e^{-\mu/2}$.

Note that Eqn. A-22 is identical with Eqn. (I.18) in Kikuchi and Brush; it is different from the corresponding set of equations (A.22) in Maren [24]. This is because the interaction enthalpy term used by Kikuch and Brush, and in this work, is $2\varepsilon_1(2y_2 - y_1 - y_3)$, and in Maren [24], the term used was the simpler $\varepsilon_1(2y_2)$. The additional factor of 2 in this work and in the original Kikuch and Brush development is used to credit each interaction between units separately; from unit X to Y and then again from Y back to X . That factor of 2 was absorbed in the previous work by Maren.

Our goal is to find the equilibrium values for each of these configuration variables in terms of *only* the enthalpy parameters. This is a fairly complex and convoluted derivation.

Our strategy will be to obtain the equilibrium expression for a single configuration variable, z_3 . Once we have that, we can use it (via substitutions and equivalence relations) to obtain the remaining configuration variables very easily.

A.5 The Configuration Variable z_3 at Equilibrium: Precursor Steps

As an illustration, we compute the term for z_3 .

To do this, we seek the dependence of the free energy on z_3 , given as

$$0 = \frac{\partial \bar{G}_{2-D}}{\partial z_3} = \frac{\partial}{\partial z_3} \left[\varepsilon_0 x_1 + 2\varepsilon_1(-z_1 + z_3 + z_4 - z_6) - \bar{S}_{2-D} \right. \\ \left. + \mu \left(1 - \sum_{i=1}^6 \gamma_i z_i \right) + 4\lambda(z_3 + z_5 - z_2 - z_4) \right]. \quad (\text{A-23})$$

We use the equivalence relation in Eqn. A-7a to identify an expression for x_1 in terms of z_3 , and so can write

$$\frac{\partial(\varepsilon_0 x_1)}{\partial z_3} = \varepsilon_0 \frac{\partial(z_1 + z_2 + z_3 + z_5)}{\partial z_3} = \varepsilon_0. \quad (\text{A-24})$$

Carrying through with the terms that are linear in z_3 , we can write

$$0 = \frac{\partial \bar{G}_{2-D}}{\partial z_3} = \varepsilon_0 + 2\varepsilon_1 - \mu + 4\lambda - \frac{\partial \bar{S}_{2-D}}{\partial z_3} \quad (\text{A-25})$$

To find the dependence of the entropy on a specific configuration variable, we first obtain the derivative of the $Lf(x)$ term.

$$\frac{\partial Lf(x)}{\partial x} = \frac{\partial [x \ln(x) - x]}{\partial x} = \ln(x). \quad (\text{A-26})$$

In order to find the specific dependence of the entropy term on z_3 , we first need to find the dependence of each of the configuration variables on z_3 .

First Step: Find the dependence of the entropy on z_3

To complete this, we need the dependence of each of the configuration variables x_i , y_i , and w_i on z_3 . Referring again to our set of equivalence relations in Eqns. A-5, A-6, and A-7, we have

$$\begin{aligned} \partial x_1 / \partial z_3 &= \partial(z_1 + z_2 + z_3 + z_5) / \partial z_3 = 1 \\ \partial x_2 / \partial z_3 &= \partial(z_2 + z_4 + z_5 + z_6) / \partial z_3 = 0 \\ \partial y_1 / \partial z_3 &= \partial(z_1 + z_2) / \partial z_3 = 0 \\ \partial y_2 / \partial z_3 &= \partial(z_3 + z_5 + z_2 + z_4) / 2\partial z_3 = 1/2 \\ \partial y_3 / \partial z_3 &= \partial(z_5 + z_6) / \partial z_3 = 0 \\ \partial w_1 / \partial z_3 &= \partial(z_1 + z_3) / \partial z_3 = 1 \\ \partial w_2 / \partial z_3 &= \partial(z_2 + z_5) / \partial z_3 = 0 \\ \partial w_3 / \partial z_3 &= \partial(z_4 + z_6) / \partial z_3 = 0 \end{aligned} \quad (\text{A-27})$$

Consulting Eqn. A-27, we see that the only configuration variables that have a dependence on z_3 are x_1 , y_2 , and w_1 . Thus,

$$\frac{\partial \bar{S}_{2-D}}{\partial z_3} = \frac{\partial}{\partial z_3} \left[2 \sum_{i=1}^3 \beta_i Lf(y_i) + \sum_{i=1}^3 \beta_i Lf(w_i) - \sum_{i=1}^2 Lf(x_i) - 2 \sum_{i=1}^6 \gamma_i Lf(z_i) \right], \quad (\text{A-28})$$

or

$$\frac{\partial \bar{S}_{2-D}}{\partial z_3} = 2 * 2\ln(y_2)(1/2) + \ln(w_1) - \ln(x_1) - 2\ln(z_3). \quad (\text{A-29})$$

Second Step: Express z_3 in terms of other configuration variables

We insert Eqn. A-29 into Eqn. A-25 to obtain

$$0 = \frac{\partial \bar{G}_{2-D}}{\partial z_3} = \varepsilon_0 + 2\varepsilon_1 - \mu + 4\lambda - [2\ln(y_2) + \ln(w_1) - \ln(x_1) - 2\ln(z_3)]. \quad (\text{A-30})$$

We set $\varepsilon_0 = 0$ for the equiprobable case, and rearrange to obtain

$$2\ln(z_3) - \mu = -2\varepsilon_1 - 4\lambda + 2\ln(y_2) + \ln(w_1) - \ln(x_1). \quad (\text{A-31})$$

We divide through by 2 to obtain

$$\ln(z_3) - \mu/2 = -\varepsilon_1 - 2\lambda + \ln(y_2) + (\ln(w_1) - \ln(x_1))/2. \quad (\text{A-32})$$

We take the exponent of both sides to obtain

$$z_3 e^{-\mu/2} = e^{-\varepsilon_1} e^{-2\lambda} y_2 (w_1/x_1)^{1/2}. \quad (\text{A-33})$$

We recall that we defined $q = e^{-\mu/2}$ and make the substitution to obtain

$$z_3 q = e^{-\varepsilon_1} e^{-2\lambda} y_2 (w_1/x_1)^{1/2}. \quad (\text{A-34})$$

Our goal has been to obtain the results previously presented in Eqn. A-22 as

$$z_3 q = e^{-2\lambda} e^{-\beta\varepsilon} y_2 (w_1/x_1)^{1/2}. \quad (\text{A-35})$$

These results are the same as those of Kikuchi and Brush, keeping in mind that we have let $\beta = 1$ and $\varepsilon_1 = \varepsilon$.

The remaining expressions in Eqn. A-22 can be similarly obtained.

A.6 Obtaining the Equilibrium Solution for the 2-D CVM

In the previous subsection, we obtained expressions for the z_i in terms of the remaining configuration variables; the x_i , y_i , and z_i . Now, we use this to find an analytic solution that gives us the equilibrium values for specific configuration variables in terms of the interaction enthalpy.

We will find it convenient to use a transformation introduced by Kikuchi and Brush (Eqn. I.23), where $h = \exp(2\beta\varepsilon_1)$. As with Kikuchi and Brush, we let $\beta = 1$. Since we are solving for the equilibrium case, we set the activation enthalpy $\varepsilon_0 = 0$. We thus simplify the notation by setting $\varepsilon_1 = \varepsilon$, so we can write $h = \exp(2\varepsilon)$.

This is a particularly long and convoluted derivation. Thus, it is labeled in terms of different steps.

Step 1: Express z_1/z_3 as the ratio s

We approach the solution given by Kikuchi and Brush (Eqn. I.25) by first letting $s = z_1/z_3$. Then

$$s = z_1/z_3 = \frac{e^\varepsilon y_1 (w_1/x_1)^{1/2}}{e^{-2\lambda} e^{-\varepsilon} y_2 (w_1/x_1)^{1/2}} \quad (\text{A-36})$$

or

$$s = e^{2\varepsilon} e^{2\lambda} \frac{y_1}{y_2} = h e^{2\lambda} \frac{y_1}{y_2}, \quad (\text{A-37})$$

where $h = \exp(2\varepsilon)$.

The Kikuch-Brush notation for the h - value

Kikuchi and Brush [2] restrict their attention to the case where the activation enthalpy parameter $\varepsilon_0 = 0$, so that there is an equiprobable distribution of units into states **A** and **B** ($x_1 = x_2 = 0.5$). In

this particular case, it is possible to find an analytic solution for ε_1 in terms of the configuration variables, and vice versa. It becomes more convenient to express the interaction enthalpy ε_1 in terms of an interaction enthalpy parameter h .

Kikuchi and Brush used the parameter replacement $h = e^{2\beta\varepsilon_1}$ (Eqn. I-23 [2]; Kikuchi and Brush use H instead of h). As we are working with the reduced equation formalism, we let $\beta = 1$, so that $h = e^{2\varepsilon_1}$. Further, since the analytic solution is specific to the case where $\varepsilon_0 = 0$, we set $\varepsilon_1 = \varepsilon$, so that $h = e^{2\varepsilon}$. Throughout this paper, and others in this series, we refer to h as the *h-value*, which is the key parameter governing the topography at a free energy minimum.

Step 2: Multiply z_1 and z_3

We next perform the multiplication of z_1q and z_3q from Eqn. A-22 to obtain

$$z_1z_3q^2 = e^\varepsilon y_1(w_1/x_1)^{1/2} * e^{-2\lambda} e^{-\varepsilon} y_2(w_1/x_1)^{1/2} \quad (\text{A-38})$$

or

$$z_1z_3q^2 = e^{-2\lambda} y_1y_2(w_1/x_1). \quad (\text{A-39})$$

Step 3: Square z_2

Next, we square the expression that we have for z_2q , so that from

$$z_2q = e^\lambda (y_1y_2w_2)^{1/2} (x_1x_2)^{-1/4} \quad (\text{A-40})$$

we obtain

$$z_2^2q^2 = e^{2\lambda} (y_1y_2w_2)(x_1x_2)^{-1/2}. \quad (\text{A-41})$$

Step 4: Reduce number of configuration variables by isolating y_1y_2

Our next step is to reduce the number of configuration variables used in the expressions for the z_1 , z_2 , and z_3 variables. We do this by

noticing that the factor of y_1y_2 occurs in both Eqns. A-39 and A-41. We isolate this term from the previous Eqn. A-41.

$$y_1y_2 = \frac{z_2^2q^2e^{-2\lambda}}{w_2}(x_1x_2)^{1/2}. \quad (\text{A-42})$$

We substitute the expression for y_1y_2 into the equation for z_1z_3 to obtain

$$z_1z_3q^2 = e^{-2\lambda}y_1y_2(w_1/x_1) = e^{-2\lambda} \left[\frac{z_2^2q^2e^{-2\lambda}}{w_2}(x_1x_2)^{1/2} \right] (w_1/x_1). \quad (\text{A-43})$$

We collect terms and divide through by q^2 on both sides to obtain

$$z_1z_3 = e^{-4\lambda}z_2^2\frac{w_1}{w_2}(x_2/x_1)^{1/2}. \quad (\text{A-44})$$

We recall that at equilibrium for $\varepsilon_0 = 0$, and we have $x_1 = x_2$ to obtain

$$z_1z_3 = e^{-4\lambda}z_2^2\frac{w_1}{w_2}. \quad (\text{A-45})$$

Following the line of thought presented by Kikuchi and Brush (Eqn. I.22), we can set $\lambda = 0$, and so write

$$z_1z_3 = z_2^2\frac{w_1}{w_2}. \quad (\text{A-46})$$

We have moved from a representation for the configuration variables that requires all of the x_i , y_i , and w_i to express the z_i to a representation for the z_i that involves only the z_i and w_i ; that is, we have removed the x_i and the y_i from the representation for the z_i .

Step 5: Represent z_2 in terms of z_1 and z_3

As a next step, we will write z_2 in terms of z_1 and z_3 .

We recall, from the *equivalence relations* presented at the beginning of this appendix, that

$$x_1 = y_1 + y_2 = z_1 + z_2 + z_3 + z_5. \quad (\text{A-47})$$

Also, since at $x_1 = 0.5$, we have $z_2 = z_5$, we rewrite the previous equation as

$$x_1 = 0.5 = z_1 + 2z_2 + z_3. \quad (\text{A-48})$$

We can express z_2 in terms of z_1 and z_3 , by writing

$$2z_2 = 0.5 - z_1 - z_3. \quad (\text{A-49})$$

We divide through by 2, and square both sides to obtain

$$z_2^2 = [0.5 - z_1 - z_3]^2/4 = [1 - 2z_1 - 2z_3]^2/16. \quad (\text{A-50})$$

We substitute this into Eqn. A-46 to obtain

$$z_1 z_3 = [1 - 2z_1 - 2z_3]^2 \frac{w_1}{16w_2}. \quad (\text{A-51})$$

Step 6: Divide through by z_3^2 ; multiply both sides by $\frac{w_2}{w_1}$

We divide through by z_3^2 and multiply both sides by $\frac{w_2}{w_1}$ to obtain

$$\frac{z_1}{z_3} \frac{w_2}{w_1} = [1 - 2z_1 - 2z_3]^2 / (16z_3^2). \quad (\text{A-52})$$

Carrying through the division by z_3^2 on the RHS and rearranging terms, we get

$$\frac{z_1}{z_3} \frac{w_2}{w_1} = [1/z_3 - 2z_1/z_3 - 2]^2 / (16). \quad (\text{A-53})$$

We previously defined $s = z_1/z_3$. We now substitute this into Eqn. A-53 to obtain

$$s \frac{w_2}{w_1} = [1/z_3 - 2s - 2]^2 / (16). \quad (\text{A-54})$$

Step 7: Express w_1 and w_2 in terms of z_3

We now need to express the fraction variables w_1 and w_2 in terms of z_3 . To do this, we recall from the *equivalence relations* that

$$w_1 = z_1 + z_3 \quad (\text{A-55})$$

$$w_2 = z_2 + z_5 \quad (\text{A-56})$$

Further, at equilibrium, $z_2 = z_5$, so we have $w_2 = 2z_2$.
 We have previously established that, at equilibrium,

$$2z_2 = 0.5 - z_1 - z_3. \quad (\text{A-57})$$

Thus, we can write

$$w_2 = 0.5 - z_1 - z_3. \quad (\text{A-58})$$

Using this expression for w_2 , as well as the expression that $w_1 = z_1 + z_3$, we make substitutions into Eqn.A-54 to obtain an expression involving only the z_i configuration variables, given as

$$s \frac{[0.5 - z_1 - z_3]}{z_1 + z_3} = [1/z_3 - 2s - 2]^2/16. \quad (\text{A-59})$$

We multiply the LHS of Eqn. A-59 through, top and bottom, by $2/z_3$ to obtain an equation that is only in terms of s and z_3 , given as

$$s \frac{[1/z_3 - 2s - 2]}{2(s+1)} = [1/z_3 - 2s - 2]^2/16, \quad (\text{A-60})$$

which we can immediately rewrite as

$$\frac{s}{(s+1)} = [1/z_3 - 2s - 2]/8. \quad (\text{A-61})$$

We now solve for s in terms of z_3 . Cross-multiplication gives

$$\frac{8s}{(s+1)} = 1/z_3 - 2s - 2, \quad (\text{A-62})$$

and we reorganize terms to rewrite as

$$1/z_3 = \frac{8s}{(s+1)} + 2(s+1). \quad (\text{A-63})$$

We bring the terms on the RHS over the common denominator of $s+1$ and write

$$1/z_3 = \frac{8s + 2(s+1)^2}{(s+1)}, \quad (\text{A-64})$$

which we can rewrite as

$$1/z_3 = \frac{2(4s + (s+1)^2)}{(s+1)} = \frac{2(4s + s^2 + 2s + 1)}{(s+1)} = \frac{2(s^2 + 6s + 1)}{(s+1)} \quad (\text{A-65})$$

Step 8: Express y_1 and y_2 in terms of z

We recall our initial definition of s in Eqn. A-37, which we simplify, knowing that we have already set $\lambda = 1$, so that we have

$$s = h e^{2\lambda} \frac{y_1}{y_2} = h \frac{y_1}{y_2}. \quad (\text{A-66})$$

We now wish to obtain an expression for y_2/y_1 in terms of s and z_3 , so we recall our *equivalence expressions* for y_1 and y_2 as

$$y_1 = z_1 + z_2 \quad (\text{A-67a})$$

$$y_2 = z_2 + z_4 = z_3 + z_5 \quad (\text{A-67b})$$

$$(\text{A-67c})$$

We also recall that at equilibrium, when $x_1 = x_2$, we also have $y_1 = y_3$ and that there are a set of equalities among the z_i , specifically that $z_3 = z_4$. We further recall Eqn. A-68, in which we expressed z_2 in terms of z_1 and z_3

$$2z_2 = 0.5 - z_1 - z_3. \quad (\text{A-68})$$

This allows us to write

$$y_1 = z_1 + z_2 = z_1 + [0.5 - z_1 - z_3]/2 \quad (\text{A-69})$$

and

$$y_2 = z_2 + z_4 = z_2 + z_3 = [0.5 - z_1 - z_3]/2 + z_3. \quad (\text{A-70})$$

and

$$y_2 = [0.5 - z_1 + z_3]/2. \quad (\text{A-71})$$

Step 9: Obtain y_2/y_1

We combine Eqns. A-69 and A-71, and multiply both top and bottom by 2, to create an expression for y_2/y_1 as

$$y_2/y_1 = \frac{0.5 - z_1 + z_3}{0.5 + z_1 - z_3} = \frac{1 - 2z_1 + 2z_3}{1 + 2z_1 - 2z_3} \quad (\text{A-72})$$

We recall the earlier Eqn. A-37 of s in terms of y_1 and y_2 , and also, from Eqn. A-36, in terms of z_1 and z_3 , where we had

$$s = e^{2\varepsilon} e^{2\lambda} \frac{y_1}{y_2} = h e^{2\lambda} \frac{y_1}{y_2} = h \frac{y_1}{y_2}. \quad (\text{A-73})$$

We rearrange to isolate h as

$$h = s \frac{y_2}{y_1}. \quad (\text{A-74})$$

We substitute the expression that we have just obtained for y_2/y_1 into this equation to obtain

$$h = s \frac{1 - 2z_1 + 2z_3}{1 + 2z_1 - 2z_3} \quad (\text{A-75})$$

We divide through, top and bottom, by z_3 , and use the expression that $s = z_1/z_3$, to obtain

$$h = s \frac{1/z_3 - 2s + 2}{1/z_3 + 2s - 2} \quad (\text{A-76})$$

We recall Eqn. A-65, which gave us the expression for $1/z_3$ as

$$1/z_3 = \frac{2(s^2 + 6s + 1)}{(s + 1)} \quad (\text{A-77})$$

We substitute from Eqn. A-77 into Eqn. A-76 to obtain

$$h = s \frac{\left[\frac{2(s^2+6s+1)}{(s+1)} \right] - 2s + 2}{\left[\frac{2(s^2+6s+1)}{(s+1)} \right] + 2s - 2} \quad (\text{A-78})$$

We multiply Eqn. A-78 through, top and bottom, by $s + 1$, and divide through by 2, to obtain

$$h = s \frac{(s^2 + 6s + 1) - (s - 1)(s + 1)}{(s^2 + 6s + 1) + (s - 1)(s + 1)} \quad (\text{A-79})$$

or

$$h = s \frac{s^2 + 6s + 1 - s^2 + 1}{s^2 + 6s + 1 + s^2 - 1} \quad (\text{A-80})$$

or

$$h = s \frac{6s + 2}{2s^2 + 6s} = \frac{3s + 1}{s + 3}. \quad (\text{A-81})$$

We now create an expression for s in terms of h , and the first step is

$$h(s + 3) = 3s + 1. \quad (\text{A-82})$$

We collect like terms and obtain

$$s(h - 3) = 1 - 3h, \quad (\text{A-83})$$

or

$$s = \frac{1 - 3h}{h - 3} \quad (\text{A-84})$$

Step 10: Obtain $1/z_3$ in terms of h

Once again, we recall Eqn. A-65

$$1/z_3 = \frac{2(s^2 + 6s + 1)}{(s + 1)}. \quad (\text{A-85})$$

We substitute our expression for s from Eqn. A-84 into Eqn. A-65 to obtain

$$1/z_3 = \frac{2}{\left(\frac{1-3h}{h-3} + 1\right)} \left[\left(\frac{1-3h}{h-3}\right)^2 + 6\frac{1-3h}{h-3} + 1 \right]. \quad (\text{A-86})$$

We multiply through, top and bottom, by $(h - 3)^2$ to obtain

$$1/z_3 = \frac{2(h-3)^2}{(h-3)((1-3h) + (h-3))} \left[\left(\frac{1-3h}{h-3}\right)^2 + 6\frac{1-3h}{h-3} + 1 \right] \quad (\text{A-87})$$

or

$$1/z_3 = \frac{2(h-3)^2}{(h-3)((-2)(h+1))} \left[\left(\frac{1-3h}{h-3}\right)^2 + 6\frac{1-3h}{h-3} + 1 \right] \quad (\text{A-88})$$

or

$$1/z_3 = \frac{(-1)}{(h-3)(h+1)} \left[(1-3h)^2 + 6(1-3h)(h-3) + (h-3)^2 \right] \quad (\text{A-89})$$

We simplify the terms on the right-hand-side to obtain

$$(1-3h)^2 = 1 - 6h + 9h^2, \quad (\text{A-90})$$

$$6(1-3h)(h-3) = 6(h-3h^2-3+9h) = -6(3h^2-10h+3) = -18h^2+60h-18, \quad (\text{A-91})$$

and

$$(h-3)^2 = h^2 - 6h + 9. \quad (\text{A-92})$$

Combining all terms, we obtain

$$(1-3h)^2 + 6(1-3h)(h-3) + (h-3)^2 = 1 - 6h + 9h^2 - 18h^2 + 60h - 18 + h^2 - 6h + 9. \quad (\text{A-93})$$

Identifying this simply as the RHS (RHS-term), we combine like terms

$$RHS = (9-18+1)h^2 + (-6+60-6)h - 18 + 1 + 9 = -8h^3 + 48h - 8 = 8(-h^2 + 6h - 1) \quad (\text{A-94})$$

We substitute this expression for the RHS back into Eqn. A-88 to obtain

$$1/z_3 = \frac{(-1)}{(h-3)(h+1)} \left[8(-h^2 + 6h - 1) \right] \quad (\text{A-95})$$

We invert Eqn. to obtain

$$z_3 = (h-3)(h+1) \frac{(-1)}{[8(-h^2 + 6h - 1)]} \quad (\text{A-96})$$

or

$$z_3 = \frac{(-h+3)(h+1)}{[8(-h^2 + 6h - 1)]} \quad (\text{A-97})$$

Success at last!

Kikuchi and Brush present, as their Eqn. (I.24)

$$\Delta = -h^2 + 6h - 1, \quad (\text{A-98})$$

and then give, as one element of their Eqn. (I.25),

$$z_3 = \frac{(-h + 3)(h + 1)}{8\Delta} \quad (\text{A-99})$$

The remaining configuration variables

It is not necessary to repeat this entire (and tedious) sequence in order to obtain the remaining configuration variables. Instead, we can simply use the equivalence relations to obtain most of the equations.

However, we do first need to obtain an expression for z_1 . A useful starting place is Eqn. A-84, which gives an expression for s in terms of h as

$$s = \frac{1 - 3h}{h - 3}. \quad (\text{A-100})$$

Since we know that $s = z_1/z_3$, and we have just obtained an expression for z_3 , it is straightforward to do the substitutions and obtain z_1 . Then, we can use the equivalence relations presented at the beginning of the Appendix to obtain the remaining configuration variables.

For completeness, these are listed below as (to be filled in) ...

B Appendix B: Computing the enthalpy interaction parameter from the h -value

If we make the assumption that the system is at equilibrium, we can estimate h using Eqn. A-36 from Appendix A; that is

$$z_1/z_3 = y_1 * h^2/y_2 \quad (\text{B-1})$$

This allows us to write h as

$$h = \sqrt{\frac{z_1 * y_2}{z_3 * y_1}} \quad (\text{B-2})$$

As an example of using this, we pick up on the discussion begun in Section ???. This discussion referenced Figure 7, which illustrates select counted (Z_1 and Z_3) and fractional (z_1 and z_3) computational variable values for an initial scale free-like grid. To compute our *target h-value*, we also need y_1 and y_2 .

To obtain the additional configuration variable values y_1 and y_2 , we refer to the original experimental results. The results summary is shown in Figure 21. This shows the results for y_1 and y_2 as well as z_1 and z_3 . The grid here is the same manually-designed scale free-like system as shown in Figure 7.

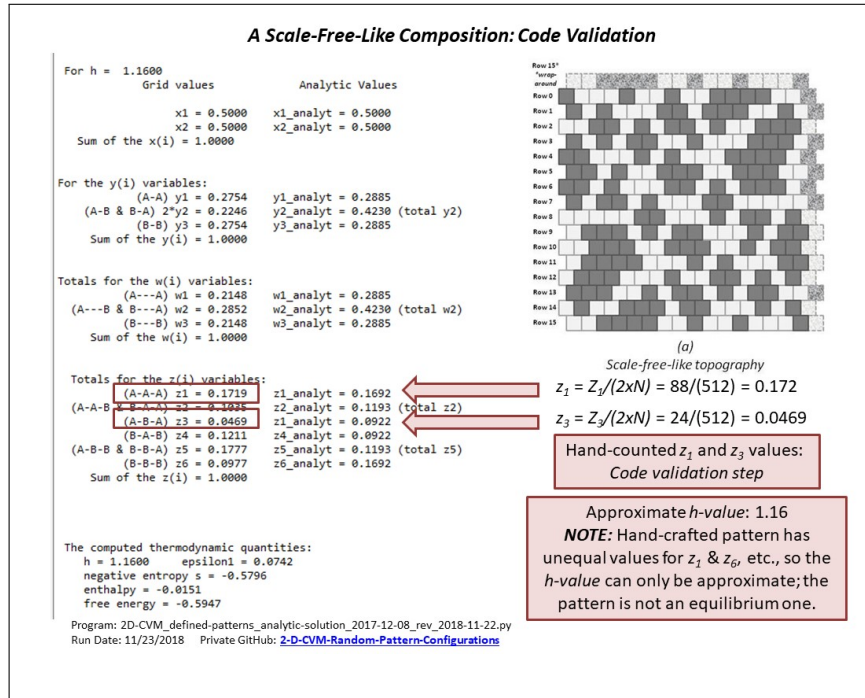


Figure 21: Configuration variable value counts for an initial manually-designed scale free-like 2-D CVM system.

These results (given in a slidedeck summarizing select experimental trials [26]) are summarized in the following Table 3.

We can visually see what the corresponding h -values are for each of the configuration variables y_2 , z_1 , and z_3 are in Figure 22.

From this, we can see some approximate h -values. There is clearly

Table 3: Configuration Variable Values for Different Values of ε_0

y_1	y_2	z_1	z_3
0.2754	0.2246	0.1719	0.0469

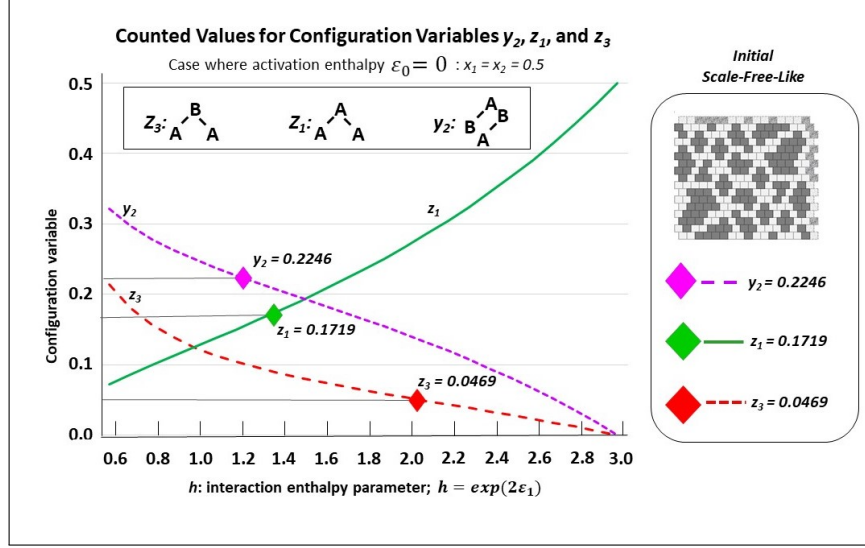


Figure 22: Configuration variable value counts for an initial manually-designed scale free-like 2-D CVM system.

a great deal of difference in the h -values corresponding to each of the different configuration variables. This is because the system is not at equilibrium.

We can take any one of several approaches to obtaining a *target* h -value. One of these methods, which we discuss here, will be to use the results from the same analytic approach as discussed previously in Appendix A, to give a computed h -value.

If we apply this approach here, we obtain

$$h = \sqrt{\frac{0.1719 * 0.2246}{0.0469 * 0.2754}} = \sqrt{2.989} = 1.729 \quad (\text{B-3})$$

This is a relatively high h -value for this system. It has obviously been skewed upwards by the very low value for $z_3 = 0.0459$.

This illustrative walk-through tells us two things. First, relying

on the analytic solution to help us obtain a useful *target h-value* is not necessarily the best approach, especially since we know that the analytic solution diverges for higher values of h .

Second, and perhaps more important, we should not blindly assume that all configuration variable values are created equal. In this illustration, the value for z_3 is associated with a much higher *h-value* than the *h-values* associated with y_1 and z_3 , respectively. (We’re not including y_1 in this discussion; we can get enough insight by looking at z_3 .)

When we look at Figure 22, we see that a reasonable *target h-value* (one that corresponds to the *h-values* for y_2 and z_1) would be in the neighborhood of $h = 1.2$. This is a relatively small *h-value*.

If we were to bring the system into equilibrium around $h = 1.2$, we would expect that the z_3 value would shift and become a bit larger. Specifically, we would expect that z_3 would increase from 0.0469 (its current value) to about 0.1.

The z_3 configuration value expresses the relative fraction of **A-B-A** triplets. One of the most obvious ways to increase z_3 is create many small “islands” “landmasses” of **A** units that are relatively close to each other. Specifically, they should be separated by narrow channels that are only one unit of **B** in width.

We can imagine what would happen if we brought this grid into a free energy-minimized state around $h = 1.2$, so that the z_3 value would increase. This would mean that we’d have more “narrow channels” between the various islands of **A** units. We might expand the boundaries of certain landmasses to reduce the distance between them.

Since z_3 is too small, compared with what we’d expect if we had $h = 1.2$, it’s interesting to take a look at the value for z_4 is also too small. Consulting the experimental results (see Figure 21, we find that $z_4 = 0.1211$. This is actually very close to what we’d expect for $h = 1.2$. In fact, it is a bit higher than what we’d expect.

The z_4 value reflects the fraction of **B-A-B** triplets. When we examine Figure 22 (or go back to the original Figure 7), we see that there are indeed many narrow “channels” of **B** units separating the islands of **A** units.

In this sense, we can see that there is some similarity between these narrow channels and the kind of naturally-occurring channels that occur in a physical topography. A good example of this would be how the English Channel separates Great Britain from France (see Figure 23).

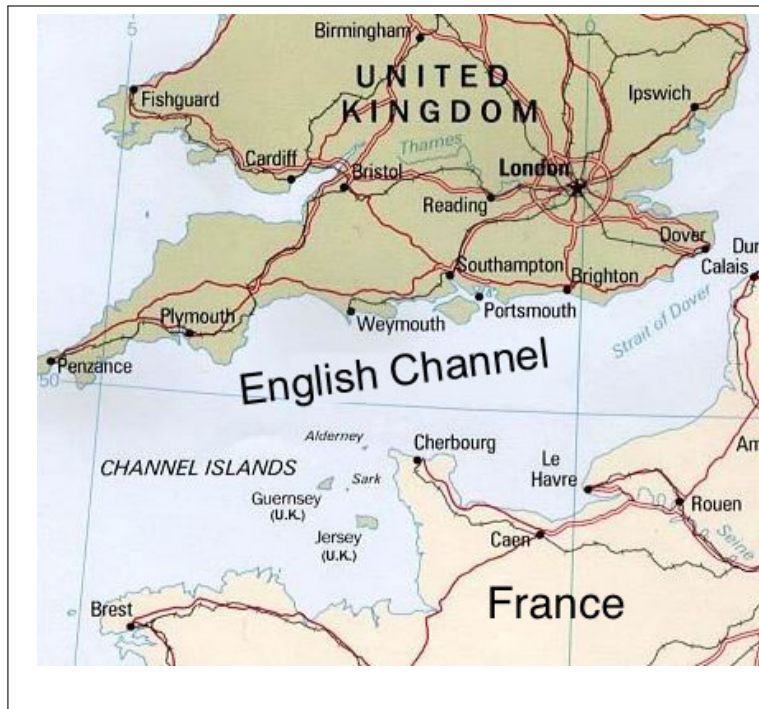


Figure 23: Illustration of a narrow channel (the English Channel) in geographic topology. Image is in the public domain, see Wikimedia for the EnglishChannel: “This image is a work of a Central Intelligence Agency employee, taken or made as part of that person’s official duties. As a Work of the United States Government, this image or media is in the public domain in the United States.”

As a contrasting discussion, we can think through what we’d expect in terms of how the topography would change if h were increased, e.g., $h = 1.65$. (This is pretty close to the h -value that we obtained via analytic solution at the beginning of this Appendix; where we found $h = 1.729$.)

When we consider natural topographies that have a relatively high “agglutinative” factor, meaning that the land coalesces largely into larger islands and landmasses, we see that there is not that much in the way of very closely-spaced little islands. Lots of little islands would be more characteristic of a lower h -value, and when we push the h -value to be less than zero, we wind up moving towards a checkerboard-like

pattern; the islands get smaller and the space between them is narrow as well.

If we increase the h -value, then we'd expect to be joining some of these islands together. That is, we'd increase z_1 (the relative fraction of **A-A-A** triplets), and decrease y_2 (the relative fraction of boundaries between unlike masses, that is, the **A-B** and **B-A** pairs).

Figure 24 shows the results of a free energy minimization trial applied to this initial grid, when we set $h = 1.65$.

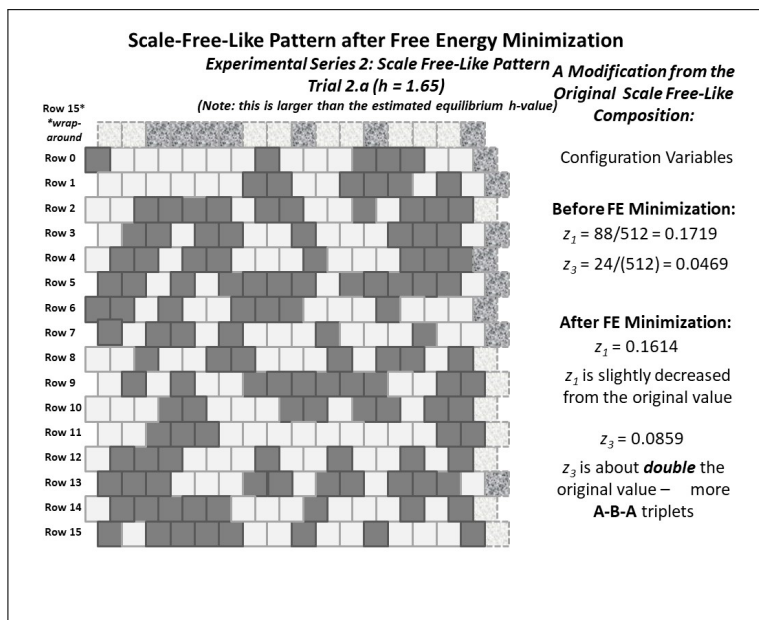


Figure 24: The result of free energy minimization applied to the initial scale-free-like grid, for $h = 1.65$.

We can see, in Figure 24, that we actually have combined many of the isolated islands into contiguous landmasses. What is particularly interesting here is that we can see several new instances of long **A-A-A** channels, increasing the z_3 value. (A good instance is in the left-hand-side of figure.)

Although z_3 is actually *increased*, we can refer back to Figure 22. Considering what has happened, we can see that the increase in z_3 is a natural and expected result; the original value was too small, even for a relatively high h -value.

In this resulting configuration, the value for z_1 is actually decreased (a little), and we would have expected a slight increase. This is most likely due to the simplistic nature of the free energy minimization algorithm; it is currently a simple random pick-and-switch process.

If we were working with a more sophisticated, topographically-sensitive free energy minimization algorithm, we would likely see that more of the islands would coagulate into landmasses. We would also likely see more “rivers” of **B** units flowing out from these landmasses of **A** units.

This suggests, of course, that it would be fascinating to characterize natural topographies using this 2-D CVM minimization process.

C Appendix C: Computing ε_0 for a given x_1 when $\varepsilon_1 = 0$

Our goal in this Appendix is to find the correlation between x_1 values and the ε_0 activation enthalpy parameter, for the case where $\varepsilon_1 = 0$.

We begin with the free energy equation, previously introduced in Section 5.2 as Eqn. 4, and repeated here for convenience as

$$\begin{aligned} \bar{F}_{2-D} = F_{2-D}/N = & \\ & \varepsilon_1(-z_1 + z_3 + z_4 - z_6) - \bar{S}_{2-D} \\ & + \mu\left(1 - \sum_{i=1}^6 \gamma_i z_i\right) + 4\lambda(z_3 + z_5 - z_2 - z_4) \end{aligned} \quad (\text{C-1})$$

We will change this equation by setting $\varepsilon_1 = 0$ and introducing the term containing the activation enthalpy ε_0 . (See Eqn. 6.) Also, since we will be taking the derivative of this equation with respect to x_1 , and we know that we will set the Lagrangian parameters equal to zero (as we did in Appendix A), we will remove them from this next iteration of the equation, giving us

$$\bar{F}_{2-D} = \varepsilon_0 x_1 - \bar{S}_{2-D} \quad (\text{C-2})$$

We take the derivative with respect to x_1

$$0 = \frac{\partial \bar{F}_{2-D}}{\partial x_1} = \varepsilon_0 - \frac{\partial}{\partial x_1} [\bar{S}_{2-D}]. \quad (\text{C-3})$$

We recall, from Eqn. 15 Subsection 5.2, our definition for \bar{S}_{2-D} as

$$\begin{aligned}\bar{S}_{2-D} = S_{2-D}/N = & \\ & 2 \sum_{i=1}^3 \beta_i Lf(y_i) + \sum_{i=1}^3 \beta_i Lf(w_i) \\ & - \sum_{i=1}^2 Lf(x_i) - 2 \sum_{i=1}^6 \gamma_i Lf(z_i),\end{aligned}\tag{C-4}$$

where $Lf(v) = v \ln(v) - v$.

We recall, from Appendix A, the derivative of $Lf(v)$ as

$$\frac{\partial Lf(v)}{\partial v} = \frac{\partial [v \ln(v) - v]}{\partial v} = \ln(v).\tag{C-5}$$

We recall, from earlier in this work, that when we had no interaction enthalpy and thus a random distribution of units into their various configurations, that the 2-D CVM entropy was the same as the basic entropy when the extra CVM (y_i , w_i , and z_i) were identical - that is, at this point, the extra configuration variables did not contribute a difference to the total 2-D CVM entropy.

Thus, for simplicity, we'll look just at the entropy involving the x_i terms.

$$\bar{S}_{2-D} = S_{2-D}/N = - \sum_{i=1}^2 Lf(x_i),\tag{C-6}$$

and thus

$$\begin{aligned}\frac{\partial}{\partial x_1} [\bar{S}_{2-D}] & \\ & = - \frac{\partial}{\partial x_1} [\ln(x_1) + \ln(1 - x_1)] \\ & = - \left[\ln(x_1) + \ln(1 - x_1) \frac{\partial}{\partial x_1} (1 - x_1) \right] \\ & = - \left[\ln(x_1) - \ln(1 - x_1) \right] = -\ln(x_1) + \ln(1 - x_1).\end{aligned}\tag{C-7}$$

We substitute this back into Eqn. C-3 to obtain

$$\varepsilon_0 = \frac{\partial}{\partial x_1} [\bar{S}_{2-D}] = \ln(x_1) - \ln(1 - x_1).\tag{C-8}$$

Table 4: Configuration Variable Values for Different Values of ε_0

ε_0	x_1	y_1	z_1	Z_1
0	0.5	0.25	0.075	19
1.0	0.269	0.0724	0.0194	5
2.0	0.119	0.0141	0.0017	0.43
3.0	0.047	0.0022	0.0001	0.03

We can obtain a very simple set of values for ε_0 from this. For example:

- $x_1 = 0.5$: $\varepsilon_0 = -\ln(0.5) + \ln(1 - 0.5) = 0$
- $x_1 = 0.269$: $\varepsilon_0 = -\ln(0.269) + \ln(0.731) = -(-1.313) + (-0.313) = 1.0$
- $x_1 = 0.119$: $\varepsilon_0 = -\ln(0.119) + \ln(0.881) = -(-2.129) + (-0.127) = 2.002$

(Note: Other values for x_1 corresponding to nominal values for ε_0 were created using interpolation.)

Table 4 identifies select configuration variable values for certain values of ε_0 . Additionally, it identifies the number of corresponding units / pairs / triplets within a 256-unit 2-D CVM grid that is designed with the corresponding value for x_1 .

From this table, it is clear that - especially if we are dealing with a small-scale 2-D CVM grid (as we are doing here for tractability), it is in our best interests to keep ε_0 relatively small; e.g. $\varepsilon_0 < 1$. When we increase the value of ε_0 much beyond that, then we run the risk of having too few active units to create even a single instance of each of the different kinds of triplets.

D Appendix D: Experimental results: configuration variables for different x_1 when varying ε_1

We are able to find the computational values for y_2 , z_1 , and z_3 (as well as others, if needed) for values of $x_1 \neq 0.5$ by following the *Protocol* briefly identified in previous sections.

Table 5: Configuration Variable y_2 Values for Different Values of ε_1 and x_1

ε_1	$x_1 = 0.5$	$x_1 = 0.35$
0.8	0.342	0.301
0.9	0.300	0.268
1.0	0.251	0.228
1.1	0.206	0.190
1.2	0.174	0.157
1.3	0.166	0.145
1.4	0.152	0.148
1.5	0.167	0.148
1.6	0.163	0.144
1.7	0.153	0.146
1.8	0.166	0.151

Table 5 presents the values for y_2 , for the cases where $x_1 = 0.5$ and $x_1 = 0.35$, as well as the analytic values for y_2 .

Figure 25 presents the same information as in Table 5.

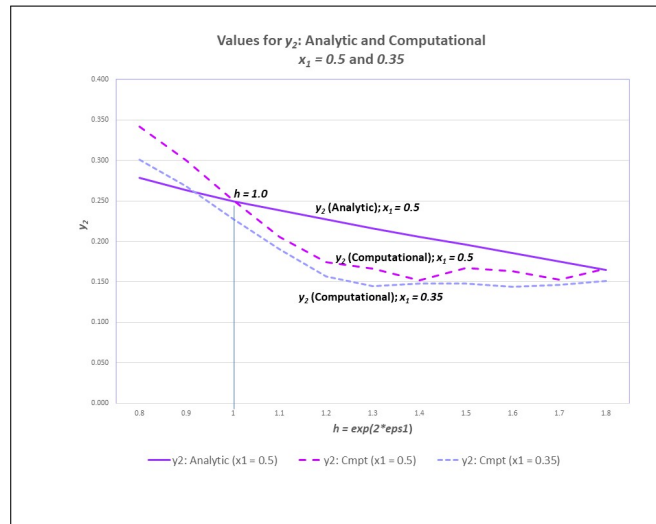


Figure 25: The y_2 values; analytic (when $x_1 = 0.5$), and computational (when $x_1 = 0.5, 0.35$ for $h = 0.8 \dots 1.8$).

The computational results are obtained by averaging the results from twenty trials for each data point.

We can see that the computational value for y_2 when $x_1 = 0.5$ is $y_2 = 0.251$, which is acceptably close to the analytic value of $y_2 = 0.250$. However, the increased values of y_2 when $h < 1.0$ (as compared with the analytic) are a bit surprising. We note that any value of $h < 1.0$ pushes in the direction of the divergence that occurs in the analytic solution when $h = 0.172$.

For convenience, we reproduce the previous Figure 13 here.

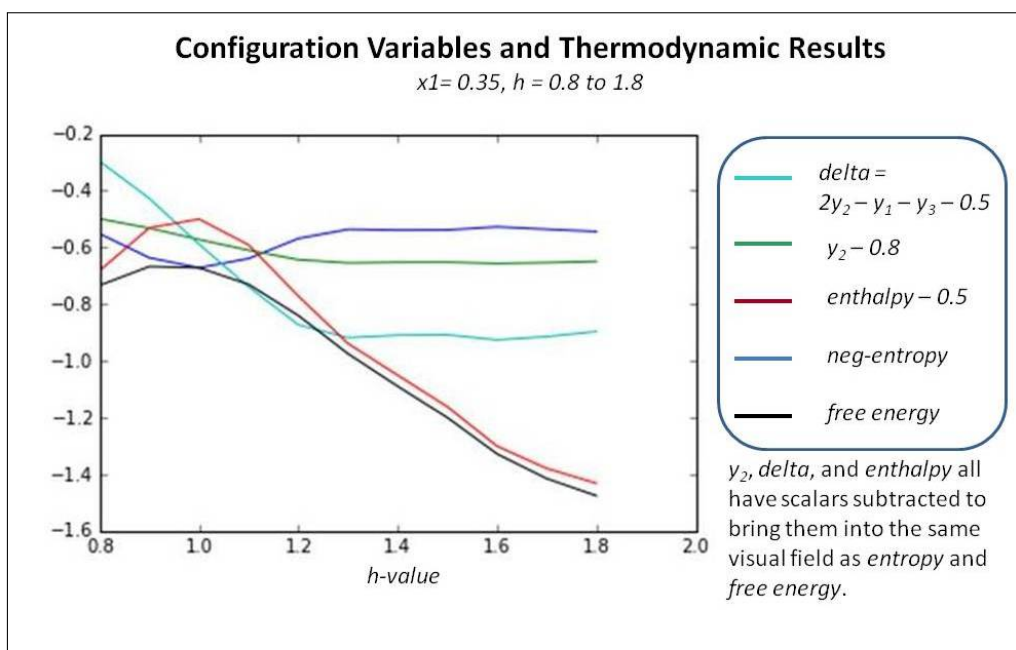


Figure 26: Configuration variable and thermodynamic values for the case where $x_1 = 0.35$ and $x_2 = 0.65$, and where the interaction enthalpy parameter h ranges as $h = 0.8..1.8$.

If we refer to Figure 26, we see that the free energy (shown in black) drops off sharply when we move to either the left or the right of $h = 1.0$. This is largely due to the influence of the enthalpy term (shown in maroon).

We get similar results for z_1 and z_3 . Table 6 gives the results for z_1 , and Figure 27 gives us visual presentation of this data.

Table 6: Configuration Variable z_1 Values for Different Values of ε_1 and x_1

ε_1	$x_1 = 0.5$	$x_1 = 0.35$
0.8	0.051	0.008
0.9	0.089	0.022
1.0	0.132	0.043
1.1	0.171	0.075
1.2	0.217	0.111
1.3	0.224	0.122
1.4	0.247	0.120
1.5	0.224	0.118
1.6	0.229	0.124
1.7	0.245	0.124
1.8	0.227	0.113

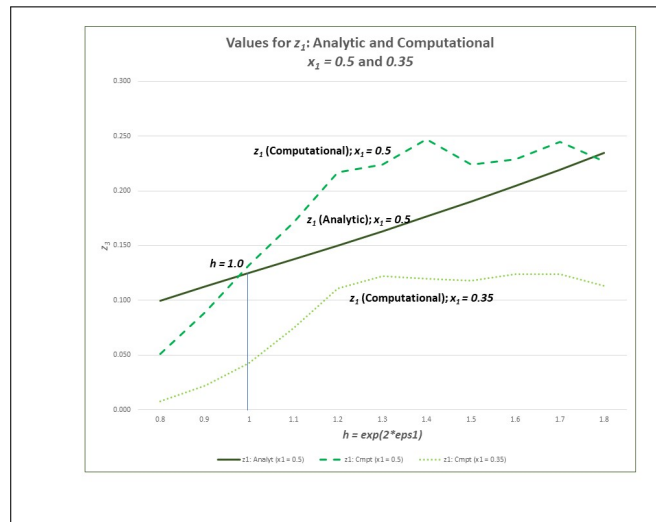


Figure 27: The z_1 values; analytic (when $x_1 = 0.5$), and computational (when $x_1 = 0.5, 0.35$ for $h = 0.8 \dots 1.8$).

Table 7 gives the results for z_3 . for z_1 , and Figure 28 gives us a similar presentation for z_3 .

Table 7: Configuration Variable z_3 Values for Different Values of ε_1 and x_1

ε_1	$x_1 = 0.5$	$x_1 = 0.35$
0.8	0.238	0.146
0.9	0.186	0.117
1.0	0.132	0.079
1.1	0.090	0.058
1.2	0.065	0.043
1.3	0.060	0.038
1.4	0.057	0.039
1.5	0.056	0.039
1.6	0.056	0.038
1.7	0.053	0.037
1.8	0.061	0.041

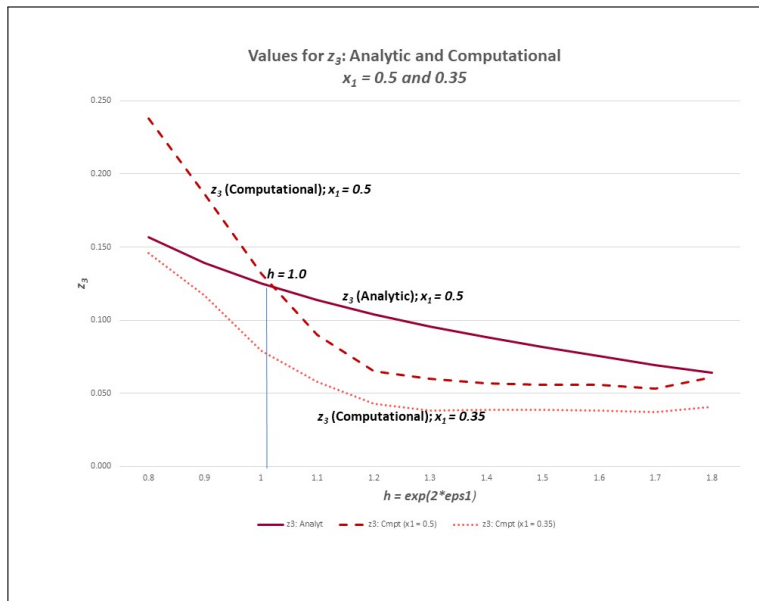


Figure 28: The z_3 values; analytic (when $x_1 = 0.5$), and computational (when $x_1 = 0.5, 0.35$) for $h = 0.8 \dots 1.8$.

References

- [1] R. Kikuchi, “A theory of cooperative phenomena,” *Phys. Rev.*, vol. 988, no. 81, p. 127–138, 1951.
- [2] R. Kikuchi and S.G. Brush, “Improvement of the cluster variation method,” *J. Chem. Phys.*, vol. 47, p. 195, 1967.
- [3] J. M. Sanchez, F. Ducastelle and D. Gratias, “Generalized cluster description of multicomponent systems,” *Physica*, vol. 128A, pp. 334-350, November, 1984. doi:10.1016/0378-4371(84)90096-7.
- [4] A.J. Maren, S.H. Lin, R.H. Langley and L. Eyring, “A theoretical model for hysteresis in solid state phase transitions,” *J. Solid State Chem.*, vol. 53, pp. 329-343, 1984. doi:10.1016/0022-4596(84)90110-5.
- [5] J.M. Sanchez and J.D. Becker, “The role of the Cluster Variation Method in the first principles calculation of phase diagrams,” *Progress of Theoretical Physics Supplement*, no. 115, pp. 131-145, 1994.
- [6] A. Pelizzola, “Cluster variation method, Padé approximants and critical behaviour,” *Phys Rev E Stat Phys Plasmas Fluids Relat Interdiscip Topics*, vol. 49, no. 4, pp. R2503-R2506, Apr., 1994.
- [7] A. Finel, “The Cluster Variation Method and Some Applications,” in P.E.A. Turchi P.E.A. and A. Gonis (eds), *Statics and Dynamics of Alloy Phase Transformations, NATO ASI Series (Series B: Physics)*, vol. 319, Springer, Boston, MA., 1994.
- [8] E.N.M. Cirillo, G. Gonnella, D.A. Johnston and A. Pelizzola, “The phase diagram of the gonihedric 3d Ising model via CVM,” *arXiv:hep-lat/9607078v1 30 Jul 1996*.
- [9] R. Kikuchi and K. Masuda-Jindo, “Cluster variation method in the computational materials science,” *Calphad*, vol. 26, no. 1, pp. 33-54, 2002. doi:10.1016/S0364-5916(02)00023-8.
- [10] T. Mohri, “Cluster variation method,” *JOM: the Journal of the Minerals, Metals and Materials Society*, vol. 65, no. 11, pp. 1510-1522, 2013. doi:10.1007/s11837-013-0738-5.
- [11] A. Pelizzola, “Cluster variation method in statistical physics and probabilistic graphical models,” *J. Phys. A: Math. Gen.*, vol. 38, p. R309, 2005. doi:10.1088/0305-4470/38/33/R01.

- [12] J.S. Yedidia, W.T. Freeman and Y. Weiss, “Understanding belief propagation and its generalizations,” *MERL TR-2001-22; Mitsubishi Electric Research Laboratories*, vol. 38, January, 2002. www.merl.com.
- [13] M.J. Wainwright and M.I. Jordan, “Graphical models, exponential families, and variational inference,” *Foundations and Trends in Machine Learning*, vol. 1, no. 1-2, pp. 1-305, 2008. doi:10.1561/2200000001.
- [14] C.A. Albers and M.A. R. Leisink and H. J. Kappen, “The cluster variation method for efficient linkage analysis on extended pedigrees,” in *BMC Bioinformatics 2006, 7(Suppl 1):S1*, vol. 38, 20 March, 2006. doi:10.1186/1471-2105-7-S1-S1.
- [15] J. Barton and S. Cocco, “Ising models for neural activity inferred via selective cluster expansion: structural and coding properties,” *J. Stat. Mech.*, vol. 03, no. P03002, pp. 1510-1522, 2013. doi:10.1088/1742-5468/2013/03/P03002.
- [16] K. Pribram, *Brain and perception: holonomy and structure in figural processing* (Hillsdale, N. J.: Lawrence Erlbaum Associates), 1991.
- [17] K. Fukushima, “Neocognitron: a self-organizing neural network model for a mechanism of pattern recognition unaffected by shift in position,” *Biol. Cybernetics*, vol. 36, pp. 193-202, 1980.
- [18] S. Grossberg and E. Mingolla, “Neural dynamics of perceptual grouping: Textures, boundaries, and emergent segmentations,” *Perception and Psychophysics*, vol. 38, pp. 141-171, 1985.
- [19] S. Grossberg and E. Mingolla, “Neural dynamics of form perception: Boundary completion, illusory figures, and neon color spreading,” *J. Psychological Review*, vol. 92, pp. 173-211, 1985.
- [20] A.J. Maren, E. Schwartz, and J. Seyfried, “Configurational entropy stabilizes pattern formation in a hetero-associative neural network,” in *Proc. IEEE Int’l Conf. SMC* (Chicago, IL), pp. 89–93, October 1992. doi:10.1109/ICSMC.1992.271796.
- [21] A.J. Maren, “Free energy as driving function in neural networks,” in *Symposium on Nonlinear Theory and Its Applications* (Hawaii), December 5-10 1993. doi:10.13140/2.1.1621.1529.
- [22] E. Schwartz and A.J. Maren, “Domains of interacting neurons: a statistical mechanical model,” in *Proc. World Congress on Neural Networks (WCNN)*, 1994. doi:10.1109/ICSMC.1992.271796.

- [23] A.J. Maren, “The cluster variation method: a primer for neuroscientists,” *Brain Sciences*, vol. 6, no. 4, p. 44, 2016.
- [24] A. Maren, “The Cluster Variation Method II: 2-D grid of zigzag chains: Basic theory, analytic solution and free energy variable distributions at midpoint ($x_1 = x_2 = 0.5$),” Tech. Rep. THM TR2014-003 (ajm), Themasis, 2014. doi:10.13140/2.1.4112.5446.
- [25] A.J. Maren, “Free Energy Minimization Using the 2-D Cluster Variation Method: Initial Code Verification and Validation,” *Themasis Technical Report 2018-001v2 (ajm)*. v1: 2018; v2: 2019. arXiv:1801.08113v2 [cs.NE] 25 Jun 2019.
- [26] A.J. Maren, “2-D cluster variation method: Comparison of Computational and Analytic Results,” June, 2019. *GitHub: github.com/ajmaren/2D-Cluster-Variation-Method; MS (TM) PPT Slidedeck: 2D-CVM-Expts-vary-eps0-and-eps1-computational-2019-06-17v4.pptx*.
- [27] K. Friston, “The free-energy principle: a unified brain theory?,” *Nat. Rev. Neurosci.*, vol. 11, pp. 127–138, 2010. doi:10.1038/nrn2787.
- [28] K. Friston, “Life as we know it,” *Journal of The Royal Society Interface*, vol. 10, no. 86, 2013.
- [29] K. Friston, M. Levin, B. Sengupta, and G. Pezzulo, “Knowing one’s place: a free-energy approach to pattern regulation,” *J. R. Soc. Interface*, vol. 12, p. 20141383, 2015. doi:10.1098/rsif.2014.1383; available online at: <http://dx.doi.org/10.1098/rsif.2014.1383>.
- [30] M. J. Beal, *Variational algorithms for approximate Bayesian inference*. PhD thesis, University College London, 2003. PDF: <http://www.cse.buffalo.edu/faculty/mbeal/papers/beal03.pdf>.
- [31] A.J. Maren, “Derivation of the variational Bayes equations,” Tech. Rep. THM TR2019-001v4 (ajm), Themasis, *arXiv:1906.08804v3 [cs.NE]* 26 Jun 2019, 2019.